[15] Bilder GE, Siegl PK, Schofield TL, Friedman PA. Chronotropic stimulation: a primary effector for release of atrial natriuretic factor. Circ Res 1989;64:799–805.

[16] Marumo F, Sakamoto H, Ando K, Ishigami T, Kawakami M. A high sensitive radioimmunoassay of atrial natriuretic peptide (ANP) in human plasma and urine. Biochem Biophys Res Commun 1986;137: 231–6.

[17] Baron A, van Bever L, Monnier D, Roatti A, Baertschi AJ. A novel K_{ATP} current in cultured neonatal rat atrial appendage cardiomyocytes. Circ Res 1999;85:707–15.

[18] Kangawa K, Tawaragi Y, Oikawa S, Mizuno A, Sakuragawa Y, Nakazato H, et al. Identification of rat gamma atrial natriuretic polypeptide and characterization of the cDNA encoding its precursor. Nature 1984;312:152–5.

[19] Vuolteenaho O, Arjamaa O, Ling N. Atrial natriuretic polypeptides (ANP): rat atria store high molecular weight precursor but secrete processed peptides of 25–35 amino acids. Biochem Biophys Res Commun 1985;129:82–8.

[20] Yan W, Wu F, Morser J, Wu Q. Corin, a transmembrane cardiac serine protease, acts as a pro-atrial natriuretic peptide-converting enzyme. Proc Natl Acad Sci U S A 2000;97:8525–9.

[21] Laine M, Arjamaa O, Vuolteenaho O, Ruskoaho H, Wechstrom M. Block of stretch-activated atrial natriuretic peptide secretion by gadolinium in isolated rat atrium. J Physiol 1994;480:553–61.

[22] Tavi P, Han C, Weckstrom M. Mechanisms of stretch-induced changes in $[Ca^{2+}]_i$ in rat atrial myocytes: role of increased troponin C affinity and stretch-activated ion channels. Circ Res 1998;83:1165–77.

[23] Schiebinger RJ, Li Y, Cragoe Jr EJ. Calcium dependency of frequency-stimulated atrial natriuretic peptide secretion. Hypertension 1994;23:710–6.

[24] Suzuki E, Hirata Y, Kohmoto O, Sugimoto T, Hayakawa H, Matsuoka H, et al. Cellular mechanisms for synthesis and secretion of atrial natriuretic peptide and brain natriuretic peptide in cultured rat atrial cells. Circ Res 1992;71:1039–48.

[25] Baxter GF. The natriuretic peptides. Basic Res Cardiol 2004;99:71–5.

[26] Ahluwalia A, MacAllister RJ, Hobbs AJ. Vascular actions of natriuretic peptides: cyclic GMP-dependent and -independent mechanisms. Basic Res Cardiol 2004;99:83–9.

[27] Rastegar MA, Vegh A, Papp JG, Parratt JR. Atrial natriuretic peptide reduces the severe consequences of coronary artery occlusion in anaesthetized dogs. Cardiovasc Drugs Ther 2000;14:471–9.

[28] Oliver PM, Fox JE, Kim R, Rockman HA, Kim HS, Reddick RL, et al. Hypertension, cardiac hypertrophy, and sudden death in mice lacking natriuretic peptide receptor A. Proc Natl Acad Sci U S A 1997;94: 14730–5.

[29] Hodgson DM, Zingman LV, Kane GC, Perez-Terzic C, Bienengraeber M, Ozcan C, et al. Cellular remodeling in heart failure disrupts K_{ATP} channel-dependent stress tolerance. EMBO J 2003;22:1732–42.

Plasma low-density lipoprotein reduction and structural effects on coronary atherosclerotic plaques by atorvastatin as clinically assessed with intravascular ultrasound radio-frequency signal analysis: A randomized prospective study

Masaki Yokoyama, MD,[a] Nobuyuki Komiyama, MD, PhD,[b] Brian K. Courtney, MD, PhD,[c] Takashi Nakayama, MD,[a] Susumu Namikawa, MD, PhD,[a] Nehiro Kuriyama, MD, PhD,[a] Tomomi Koizumi, MD, PhD,[a] Mizuo Nameki, MD, PhD,[d] Peter J. Fitzgerald, MD, PhD,[c] and Issei Komuro, MD, PhD[a] *Saitama, Japan*

Background Plaque stabilization by statins is important for reduction of cardiovascular events but has not been demonstrated enough in vivo. We examined whether statins clinically alter the structure of coronary atherosclerotic plaques using intravascular ultrasound (IVUS) radio-frequency (RF) signal analysis.

Methods Fifty consecutive patients undergoing percutaneous coronary intervention were enrolled. Intravascular ultrasound radio-frequency signals were acquired from non–percutaneous coronary intervention-targeted echolucent plaques. The patients were randomly assigned into 2 groups: group S (n = 25) taking atorvastatin 10 mg/d and group C (n = 25) as control. After 6-month follow-up, IVUS-RF signals were sampled at the same plaque sites. Several regions of interest were placed on each plaque. Intravascular ultrasound radio-frequency parameters were blindly calculated in all regions of interests (group S, n = 148; group C, n = 191). Targeted plaque volumes were also measured. Those data were compared between baseline and follow-up.

Results In group S after 6 months, plasma low-density lipoprotein level was significantly decreased (133 ± 13 to 87 ± 29 mg/dL, $P < .0001$), integrated backscatter of IVUS-RF signals was substantially increased (−53.8 ± 4.5 to −51.2 ± 4.9 dB, $P < .0001$), and plaque volume was significantly reduced, whereas no change was demonstrated in group C.

Conclusions These results suggest that statins alter properties as well as volumes of coronary plaques within 6 months, which may be related to plasma low-density lipoprotein reduction. Intravascular ultrasound radio-frequency signal analysis may be useful to evaluate the effects of drugs on stabilization of coronary atherosclerotic plaques. (Am Heart J 2005;150:287.e1-287.e7.)

The rupture of lipid-laden coronary plaques has been put forth as a frequent cause of acute coronary syndrome.[1] Because the so-called vulnerable coronary plaque frequently exists at angiographically mild or minimally stenosed sites, it is important to evaluate plaque properties and to stabilize the vulnerable plaque even in the angiographically mild stenosis.[2] Lipid-lowering therapy with statins has been proposed to affect the stability of coronary atherosclerotic plaques. Several large trials reported that statins could reduce coronary events in both primary and secondary prevention efforts.[3-9] Studies focused on coronary plaque regression with statins demonstrated that the clinical benefits of avoiding serious cardiac events are more significant than the regression of angiographically detected stenoses.[10] In rabbit studies, statins increased collagen content and decreased lipid deposition, macrophage accumulations, and matrix metalloproteinase activity in an established atheroma.[11,12] All these results suggest that statins do not only reduce plaque size but also stabilize plaques; however, the effect of statins on the histologic composition of human coronary plaque has not been well demonstrated in vivo.

Although conventional intravascular ultrasound (IVUS) imaging can provide real-time cross-sectional gray-scale images of coronary endovascular structures including plaque distribution, it is difficult to accurately identify coronary plaque subtypes such as fatty or fibrous plaques using IVUS gray-scale images.[13,14] We have reported that IVUS radio-frequency (RF) signal analysis is useful to discriminate between fibrous and degenerated tissue in vivo with >90% sensitivity and specificity.[15] In addition, several ex vivo analyses have demonstrated that IVUS-RF parameters such as integrated backscatter (IB) and other RF spectral data are useful to discriminate histologic components in a human coronary plaque.[13,16,17] In the present study, we examined whether statins clinically alter the composition of coronary atherosclerotic plaques of humans by in vivo IVUS-RF analysis.

Methods
Study design and patients
Fifty consecutive patients with stable angina indicated to percutaneous coronary intervention (PCI) were enrolled. Basic inclusion criteria were age <75 years, plasma total cholesterol (TC) level between 170 and 230 mg/dL, and without previous medical treatment of hyperlipidemia. The subjects were randomly assigned into 2 groups: group S consisted of 25 patients taking 10 mg/d of atorvastatin and group C consisted of 25 patients with only dietary modification as controls. The 10 mg/d of atorvastatin to treat hyperlipidemia is a usual and effective dosage for Japanese patients with less body mass than Americans or Europeans. Intravascular ultrasound and RF sampling were performed after PCI, but before randomization, for baseline measurements and again at 6-month follow-up. The patients were seen every month in an outpatient clinic at the Chiba University Hospital.

At baseline, we used IVUS to search for echolucent plaques with IVUS defined by the American College of Cardiology Clinical Expert Consensus Document in the PCI-targeted vessel and other non–PCI-targeted vessels.[18] Candidate plaques were required to demonstrate <50% stenosis by angiographic measurements. Plaques within the arterial segment 10 mm proximal of the PCI-targeted area were excluded to avoid influence on them from the PCI treatment. A total of 71 plaques were targeted for IVUS-RF analysis.

Major exclusion criteria were significant left main disease, unstable angina or acute myocardial infarction within the previous 3 months, or an ejection fraction <40%. Written consent was obtained from each patient for the study and the trial was approved by the institutional review board at Chiba University Hospital and the ethical committee of Chiba University Graduate School.

Intravascular ultrasound imaging and RF sampling
For all IVUS examinations, we used a ClearView Ultra IVUS system (Boston Scientific Corp, Fremont, Calif) with a 3F 40-MHz mechanical transducer catheter (Boston Scientific Corp). After intracoronary injection of nitroglycerin (0.1 mg into right coronary artery and 0.2 mg into left coronary artery),

the IVUS catheter was advanced to the distal portion of the coronary vessel. Motorized pullback of the IVUS catheter was performed at a speed of 0.5 mm/s. Intravascular ultrasound images were recorded in S-VHS videotapes during all IVUS imaging and RF sampling.

Radio-frequency signals were sampled at a single cross section through each target plaque, whereas the IVUS images were simultaneously monitored on an IVUS video screen to confirm the RF sampling sites. The cross section was basically at the site of the largest plaque area within the target plaque. Those RF signals were unprocessed "raw" signals that were completely separated from producing IVUS gray-scale images. The RF signals were digitized at 500 MHz with 8-bit resolution in an online PC with a high-speed A/D converter board (Gage Applied, Inc, Montreal, Canada) and were stored in the PC for subsequent off-line RF analysis. Radio-frequency sampling occurred during the diastolic phase of the cardiac cycle using an electrocardiogram monitor to avoid the influence of cyclic variation of the signals. The position of catheter during RF sampling was recorded by angiography. When RF signals were sampled at 6-month follow-up, extraordinary attention was paid to position an IVUS catheter at the longitudinally and circumferentially same section in the targeted plaque as baseline by using angiography or topographic landmarks of the IVUS video images, as well as distance measurements from major landmarks. Just after RF sampling, the specific profile of RF-signal amplitude related to distance from each catheter-transducer was measured in vitro using a special water tank with a polished glass plate.

Intravascular ultrasound and RF signal analysis
Volumetric measurements and calculation of RF parameters were performed by an experienced IVUS investigator (MY) blinded to treatment assignment while visualizing the baseline and follow-up IVUS video images side by side. Plaque area was measured with a planimetry software TapeMeasure (Indec Co, Sunnyvale, Calif) at 1-mm intervals from 5 mm distal to 5 mm proximal of the RF sampling site. Plaque area was defined as external elastic membrane (EEM) area minus lumen area. Plaque volume was calculated by Simpson's method of integration of the 1-mm-thick disks over the 10 serial plaque areas. Of 71 IVUS targeted plaques, 59 plaques underwent volumetric measurement, whereas accurate IVUS measurements were technically difficult for the remaining 12 plaques because of large calcifications or branch vessels. To assess the reproducibility of IVUS measurements, baseline images of 16 cases were randomly selected and reanalyzed at least 4 weeks after the initial reading. The intraobserver correlation coefficients for plaque volume, lumen volume, and vessel volume were 0.996, 0.998 and 0.998, and the percentage of errors were 0.26% ± 1.06%, 0.51% ± 1.01%, and 0.40% ± 0.86%, respectively.

Each RF data set was composed of 256 vectors over 360° of rotation of the transducer with 4096 samples per vector. A single cross-sectional image was reconstructed. Plaque area was defined as the area between the EEM and the lumen border. The plaque area was divided into 12 regions of interest (ROIs). These ROIs were automatically delineated by the custom-developed software, which divided the plaque area into sectors by using equally spaced radial lines from the center of EEM area (Figure 1).

Figure 1
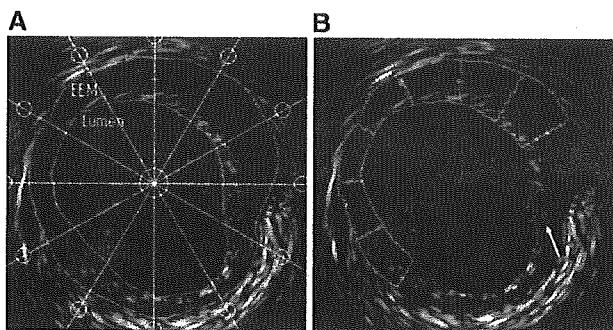
External elastic membrane and lumino-intimal border are lined on 2-dimensional mapping of RF data. Plaque area is divided into 12 ROIs with radial lines shown in panel **A**. Only ROIs with adequate thickness (>0.5 mm) and ROIs without calcification or guidewire artifact (arrow head) are selected for analysis (panel **B**).

Regions of interest with any calcifications, guidewire artifacts, or with a maximal plaque thickness of <0.5 mm were abandoned. In each ROI, time-domain statistical parameters of mean-to-SD ratio (MSR) and skewness, and a frequency-domain power parameter of IB in decibels were calculated in a PC using an originally developed software. Before calculations, the amplitude of the RF signals was corrected by the amplitude-distance profile of each specific catheter-transducer obtained just after each RF sampling procedure. The statistical parameters were based on the probability distribution function of the RF amplitude derived from an envelope of an RF signal. Skewness is the third-order parameter referring to the asymmetry of the distribution. The frequency-domain power parameter was derived from a power spectrum calculated by fast Fourier transformer. The value of IB power in an ROI was calculated according to the following equation:

$$IB = 10 \times \log_{10}(APtissue/Apref) \ (dB)$$

where APtissue is the average power (square volts) in a frequency range of 20-dB bandwidth of a signal from a tissue and APref (square volts) from a polished glass plate as a perfect reflector. The ROIs of each plaque site were matched with their corresponding ROIs at follow-up. Each of the RF parameters was compared between the matched pairs of ROIs at baseline and follow-up. In addition, IB was calculated for sliding windows with 128 data points on each vector of RF signal and presented as a color-coded 2-dimensional map, which was superimposed to a corresponding IVUS cross-sectional image. Those calculations and analysis were made by an investigator (MY) blinded to treatment assignment (by SN and MN) and independently of acquisition of IVUS images and RF signals (by NK).

To assess the reproducibility of RF parameter measurements, the investigator (NK) acquired IVUS images and RF signals at the same sites in 2 independent IVUS procedures during PCI in additional 10 patients who were randomly selected. Another investigator (MY) placed 75-paired ROIs in 10-paired plaque

areas on the reconstructed cross-sectional images acquired in the 2 procedures and calculated the RF parameters in each ROI. The correlation coefficients between the 2 RF sampling and calculating procedures for IB, MSR, and skewness in the paired ROIs were 0.991, 0.972 and 0.982, and the percentage of errors were 0.39% ± 9.78%, 0.57% ± 5.10%, and −1.43% ± 7.81%, respectively.

Statistical analysis

Values are presented as mean ± SD. Statistical analysis was performed with paired t test to compare data between baseline and follow-up, unpaired t test to compare data between groups S and C, or analysis of variance (post hoc Bonferroni) to compare IB changes among 3 classes of % low-density lipoprotein (%LDL) reduction using a commercially available software (StatView version 5.0, ABACUS Inc, Berkley, Calif). A P value <.05 was considered to be significant.

Results

Characteristics of the patients

Of the 50 patients, 8 patients were withdrawn prematurely because of a drug-related increase of serum creatinine level (1 in group S), because of re-PCI for re-stenosis before 6 months, which influenced target plaques (2 in group S and 1 in group C), and because of failure of follow-up for 6 months (2 in group S and 2 in group C). There were no complications resulting from IVUS imaging procedures.

Both groups showed no significant difference with regard to baseline characteristics including clinical histories, concomitant medications, nature of coronary artery disease, the number of studied plaques located in the PCI-targeted artery, and plasma lipid levels (Table I, Figure 2).

Effects on plasma lipid levels

The effects of atorvastatin on plasma lipid levels in 6 months are presented in Figure 2. Atorvastatin induced a marked reduction in TC and LDL cholesterol (LDL-C) levels (198 ± 17 to 156 ± 26 mg/dL and 133 ± 13 to 87 ± 29 mg/dL, respectively, $P < .0001$), whereas high-density lipoprotein cholesterol (HDL-C) level was significantly increased (44 ± 11 to 49 ± 15 mg/dL, $P = .019$) during the 6 months. Percentage of change of TC and LDL during the follow-up ([value at follow-up − value at baseline] / value at baseline × 100 [%]) in group S were −20% ± 17% and −34% ± 20%, respectively. No significant change in TC, LDL-C, and HDL-C levels was observed in group C.

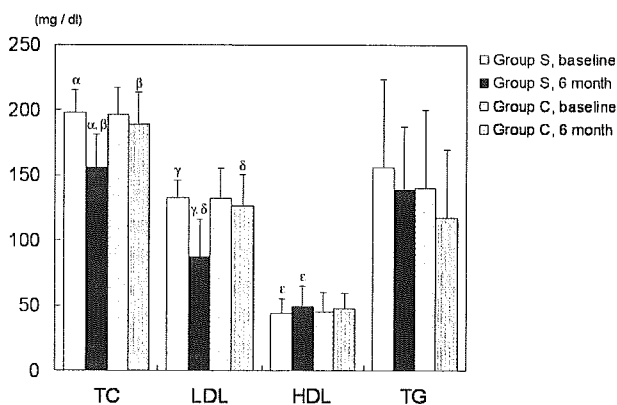### Changes in IB, MSR, and skewness over 6 months

To elucidate whether the atorvastatin treatment changes properties of coronary plaque, we compared RF parameters of 148 ROIs in group S and 191 ROIs in group C (Table II). Mean-to-SD ratio was significantly decreased (1.20 ± 0.30 to 1.14 ± 0.29,

Table I. Baseline characteristics of the patients

Variable	Group S	Group C
n	20	22
Age (y)	62.1 ± 10.2	64.4 ± 8.7
Male sex	18 (90)	20 (91)
Clinical history		
Hypertension	11 (55)	10 (45)
Diabetes mellitus type 2	3 (15)	5 (23)
Current smoking	6 (30)	7 (32)
Concomitant medications		
Aspirin	19 (95)	21 (95)
ACE inhibitor	7 (35)	8 (36)
Angiotensin antagonist	7 (35)	6 (27)
β-Blocker	7 (35)	4 (18)
Calcium antagonist	9 (45)	8 (36)
Nature of coronary artery disease		
Single vessel	18 (90)	19 (86)
Multivessel	2 (10)	3 (14)
Plaques for IVUS measurements (n)	35	36
Location of plaques for IVUS measurements		
LCA	28 (80)	29 (81)
RCA	7 (20)	7 (19)
Plaques in PCI-targeted vessel	16 (46)	19 (53)

Values are mean ± SD or number (percentage) unless otherwise indicated.
ACE, Angiotensin-converting enzyme; LCA, left coronary artery; RCA, right coronary artery.

Table II. Radio-frequency parameters derived from IVUS measurements

Parameter	Group S (n = 148)	Group C (n = 191)	P
IB			
Baseline (dB)	−53.8 ± 4.5	−53.1 ± 4.0	.184
6-m follow-up (dB)	−51.2 ± 4.9	−53.1 ± 4.8	.0001
P	<.0001	.991	
Baseline	1.86 ± 0.79	1.96 ± 1.10	.255
6-m follow-up	2.11 ± 0.78	1.94 ± 0.75	.038
P	.025	.845	
MSR			
Baseline	1.20 ± 0.30	1.24 ± 0.30	.088
6-m follow-up	1.14 ± 0.29	1.21 ± 0.26	.001
P	.040	.298	

Values are mean ± SD.

Figure 3
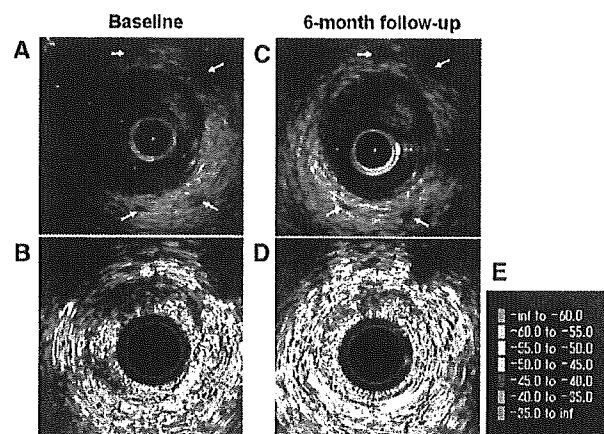
Intravascular ultrasound gray-scale cross-sectional images (upper panels) and color-coded maps reconstructed according to IB values of a coronary plaque (lower panels) in group S are shown. Panels **A** and **B** are at baseline and panels **C** and **D** are at 6-month follow-up. White arrowheads show side branches as landmarks in **A** and **C** to perform IVUS acquisitions at the same section at baseline and at 6-month follow-up. Color codes corresponding to ranges of IB value in decibels are shown in **E**. Integrated backscatter ranges became greater at 10 to 2 o'clock in the plaque area at the follow-up (panel **D**) than at baseline (panel **B**).

Figure 2

Changes in lipid parameters during the 6-month follow-up in groups S and C are shown. TC and LDL-C are significantly decreased and HDL-C is substantially increased in group S ($^{\alpha,\gamma}P$ < .0001, $^{\beta,\delta}P$ < .001, $^{\epsilon}P$ = .019). TG, Triglyceride.

P = .040) and skewness was substantially increased (1.86 ± 0.79 to 2.11 ± 0.78, P = .025) during the 6-month follow-up in group S, whereas there was no significant change in those parameters in group C. Integrated backscatter was significantly increased by 2.6 dB (−53.8 ± 4.5 to −51.2 ± 4.9 dB, P < .0001) in group S but not in group C. The increase of IB in group S could be more clearly recognized by comparison of the color-coded IB maps between baseline and follow-up (Figure 3).

The relation between IB changes and LDL changes over 6 months in group S

There was a good inverse correlation between change of LDL and change of IB values. An increase in IB change was related to %LDL reduction (LDL at baseline − LDL at

Figure 4
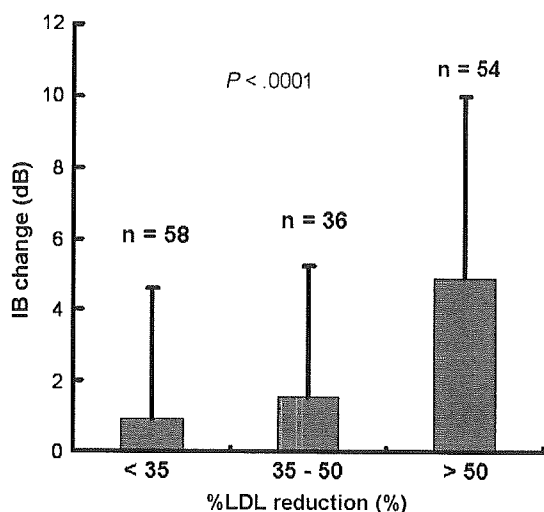
Relation between IB change in ROIs and %LDL reduction during 6 months is demonstrated. The difference of IB change was especially apparent when %LDL reduction was >50%.

Table III. Volume parameters derived from IVUS measurements

	Group S (n = 29)	Group C (n = 30)
Vessel volume		
Baseline (mm³)	135.5 ± 57.9	102.4 ± 48.1
6-m follow-up (mm³)	131.1 ± 52.8	102.5 ± 50.1
P	.194	.962
Lumen volume		
Baseline (mm³)	65.7 ± 27.8	46.6 ± 24.3
6-m follow-up (mm³)	65.0 ± 25.5	48.3 ± 29.5
P	.816	.408
Plaque volume		
Baseline (mm³)	69.9 ± 35.0	55.8 ± 27.5
6-m follow-up (mm³)	66.0 ± 32.1	53.8 ± 25.5
P	.024	.254

Values are mean ± SD.

follow-up / LDL at baseline ×100 [%]) (IB changes 0.92 ± 3.70, 1.56 ± 3.66, 4.91 ± 5.10 dB at %LDL reductions <35, 35-50, >50%, respectively, $P < .0001$). The difference of IB change was most apparent when %LDL reduction was >50% (Figure 4).

Intravascular ultrasound analysis of plaque volumes

Plaque volume was significantly reduced by 3.2% (69.9 ± 35.0 to 66.0 ± 32.1 mm³, $P = .024$) during the 6 months in group S; however, no significant change was observed in group C. Vessel volume tended to be reduced by 2.9% (135.5 ± 57.9 to 131.1 ± 52.8 mm³, $P = .194$) in group S (Table III). These results suggest that 6-month treatment with atorvastatin may reduce volumes of coronary atherosclerotic plaques.

Discussion

In the present study, atorvastatin treatment for 6 months induced changes in the acoustic properties of coronary plaques. The correlations between the value of RF parameters and tissue types in atherosclerotic plaques have been shown in several in vivo and ex vivo studies.[13-17] We have already reported that the IVUS-RF parameters were useful to discriminate between American Heart Association type III and type IV/Va human coronary plaques ex vivo.[13] In an in vivo study analyzing tissue samples resected at directional coronary atherectomy, we demonstrated that IB and skewness values were significantly greater in fibrous tissue than in degenerated tissue and that MSR values were

substantially smaller in fibrous tissue than in degenerated tissue.[15] Kawasaki et al[16] reported that IB value was significantly greater in fibrous tissue than in lipid cores by an ex vivo comparison with plaque histology. Fibrous tissues in a coronary plaque contain more collagen fibers, which may reflect RF more than fatty tissues and lead to greater IB values. Furthermore, variance of reflected RF amplitude from each fine tissue component may become greater in fibrous tissue than fatty/degenerated tissue so that it may cause the difference of MSR and skewness between fibrous tissue and fatty/degenerated tissue. Although those studies suggest that sensitive and specific IVUS-RF analysis could discriminate between fibrous and fatty tissues, complete in vivo discrimination of plaque composition is difficult because the classification of fibrous, fibro-fatty, or fatty tissues is an attempt to categorize a continuous spectrum of tissue composition to a small set of classes.[17] In the present study, RF parameters of IB and skewness were significantly increased and MSR was substantially decreased in a group treated with atorvastatin for 6 months. Lipid-lowering therapy increased collagen content and decreased lipid deposition, macrophage accumulation, and matrix metalloproteinase activity in established atherosclerotic plaques in rabbits.[11,12] These findings suggest that the changes of RF parameters reflect some combination of an increase in fibrous tissue and/or a reduction of fatty, degenerated tissue in atherosclerotic plaques.

A correlation between the degree of LDL reduction and the degree of IB change was observed in our study. Many large prevention trials with statins have shown a correlation between the percentage of reduction of cholesterol and reduction of cardiovascular events, and our results may account for the results of the large trials.[19] Schartl et al[20] demonstrated in the GAIN study that the degrees of change in acoustic properties evaluated by gray-scale echogenicity analysis of IVUS video images were significantly different between

2 groups with different degrees of lipid intervention: aggressive lipid intervention to <100 mg/dL LDL and usual lipid-lowering care over 12 months. The result is consistent with the present study. The analysis of RF ultrasound signals provides a more robust framework for this kind of inquiry than gray-scale measurements. Several more parameters can be accurately assessed with IVUS-RF as compared to gray-scale imaging, which is also machine- and user setting–dependent. This may be a reason why IVUS-RF analysis succeeded to demonstrate structural change of coronary atherosclerotic plaques by atorvastatin in a shorter period of 6 months than the previous IVUS gray-scale image analysis as in the GAIN study.

Previous clinical trials have suggested that the stabilizing effects of statin on plaques begin to take place by means of an apparently lower occurrence of ischemic events. In the WOSCOP study and the LIPID trial, according to Kaplan-Meier analysis of time to a definite nonfatal myocardial infarction or death from coronary heart disease, the cumulative risk curves begin to diverge between the pravastatin and placebo groups as early as 6 months after the initiation of treatment.[4,7] Another trial demonstrated that aggressive lipid-lowering with atorvastatin resulted in a lower ischemic event rate after 6 months compared with angioplasty.[21] The LIPS trial demonstrated that treatment with fluvastatin reduces major adverse cardiac events in patients who have undergone PCI. In this trial, major adverse cardiac events–free survival curves began to separate between fluvastatin and placebo after 6 months of follow-up.[9] Those results and observations suggest that statins stabilize coronary plaques within 6 months, which results in apparent reduction of cardiovascular events after 6 months. In addition, the present study revealed that morphologic changes of plaques occur in a relatively short time span of 6 months. The LIPS trial and our present study are similar at the point that cardiovascular events arising from lesions except plaques with severe stenosis are reduced from 6 months of statin treatment.

On the other hand, the dosage of 10 mg/d of atorvastatin in our study might be too small for American or European people to be effective for stabilizing coronary plaques as well as lipid lowering. However, the dosage for Japanese patients should be almost equivalent to a dosage of 20-80 mg/d for Euro-American people with regard to the changes of plasma lipid profiles (averaged LDL reduction of 34%) in 6 months.[19]

In the present study, plaque volume was slightly but significantly decreased after 6-month administration of atorvastatin. There are several recent reports about statin-induced volumetric change of coronary atherosclerotic plaques analyzed with IVUS video images. The REVERSAL study demonstrated that intensive lipid-lowering therapy with atorvastatin for 18 months reduced progression of coronary atherosclerosis and

plaque volume might regress especially in patients with >50% reduction of LDL-C.[22] Jensen et al reported that a significant reduction in coronary plaque volume of 6.3% was observed in patients with stable ischemic heart disease after 12-month administration of simvastatin reducing LDL-C of 42.6%.[23] The ESTABLISH study demonstrated that more reduction of plaque volume of 13.1% was observed in patients with acute coronary syndrome after 6-month administration of atorvastatin reducing LDL-C of 41.7% and suggested that unstable coronary plaques could regress more by aggressive lipid-lowering therapy.[24] Result of the present study may be almost similar to those studies. Because we selected only echolucent plaques, which might include some unstable plaques at baseline, volumetric regression in those plaques could be more easily demonstrated even after only 6-month administration of atorvastatin, reducing LDL of 34%.

In summary, the present study with IVUS-RF analysis suggests a clinically observable mechanism of structural changes as "stabilization" of coronary atherosclerotic plaques after 6-month administration of a statin.

Study limitations

There are several limitations to be taken into account in the present study. First, a small number of patients were enrolled. Second, the RF parameters analyzed in this study do not provide quantitative descriptions of the fibrous or fatty tissue components. They demonstrate trends that are believed to be highly consistent with increased fibrous composition and/or decreased lipid composition. In addition, there was no target plaque with a clearly identified lipid core, even with the use of IVUS-RF. Therefore, it was not possible to provide a validated measure of volumetric reduction of lipid cores. Third, inflammatory responses in a coronary plaque such as migration of macrophages or T lymphocytes, which is thought to be an important factor of plaque vulnerability, cannot be detected by IVUS-RF analysis method to date. Optical coherence tomography and coronary thermography are thought to be invasive diagnostic modalities that can detect and evaluate the inflammatory responses in coronary atherosclerotic plaques.[25,26] Despite these limitations, however, it was possible to observe significant changes that are consistent with known acoustic properties of important components of vascular lesions.

Conclusions

Treatment with atorvastatin altered acoustic properties of coronary atherosclerotic plaques in 6 months. These results may explain one of the mechanisms for statins to prevent ischemic coronary events demonstrated previously in large clinical trials. Intravascular ultrasound radio-frequency signal analysis may be useful

to evaluate the stabilization of coronary atherosclerotic plaques as changes of histologic composition by statin.

References

1. Falk E, Shah PK, Fuster V. Coronary plaque disruption. Circulation 1995;92:657-71.

2. Nobuyoshi M, Tanaka M, Nosaka H, et al. Progression of coronary atherosclerosis: is coronary spasm related to progression? J Am Coll Cardiol 1991;18:904-10.

3. Scandinavian Simvastatin Survival Study Group. Randomized trial of cholesterol lowering in 4444 patients with coronary heart disease. Lancet 1994;344:1383-9.

4. Shepherd J, Cobbe SM, Ford I, et al. Prevention of coronary heart disease with pravastatin in men with hypercholesterolemia. N Engl J Med 1995;333:1301-7.

5. Sacks FM, Pfeffer MA, Moye LA, et al. The effect of pravastatin on coronary events after myocardial infarction in patients with average cholesterol levels. N Engl J Med 1996;335:1001-9.

6. Downs JR, Clearfield M, Weis S, et al. Primary prevention of acute coronary events with lovastatin in men and women with average cholesterol levels: results of AFCAPS/SUB-TexCAPS. JAMA 1998;279:1615-22.

7. Long-Term Intervention with Pravastatin in Ischemic Disease (LIPID) Study Group. Prevention of cardiovascular events and death with pravastatin in patients with coronary heart disease and a broad range of initial cholesterol levels. N Engl J Med 1998;339:1349-57.

8. Riegger G, Abletschauser C, Ludwig M, et al. The effect of fluvastatin on cardiac events in patients with symptomatic coronary artery disease during one year of treatment. Atherosclerosis 1999;144:263-70.

9. Serruys PWJC, de Feyter P, Macaya C, et al. Fluvastatin for prevention of cardiac events following successful first percutaneous coronary intervention. JAMA 2002;287:3215-22.

10. Gotto AM. Lipid lowering, regression, and coronary events. A review of the Interdisciplinary Council on Lipids and Cardiovascular Risk Intervention, Seventh Council Meeting. Circulation 1995;92:646-56.

11. Shiomi M, Ito T, Tsukada T, et al. Reduction of serum-cholesterol levels alters lesional composition of atherosclerotic plaques: effects of pravastatin sodium on atherosclerosis in mature WHHL rabbits. Arterioscler Thromb Vasc Biol 1995;15:1938-44.

12. Aikawa M, Rabkin E, Okada Y, et al. Lipid lowering by diet reduces matrix metalloproteinase activity and increases collagen content of rabbit atheroma. Circulation 1998;97:2433-44.

13. Komiyama N, Berry GJ, Kolz ML, et al. Tissue characterization of atherosclerotic plaques by in intravascular ultrasound radiofrequency signal analysis: an in vitro study of human coronary arteries. Am Heart J 2000;140:565-74.

14. Prati F, Arbustini E, Labellarte A, et al. Correlation between high frequency intravascular ultrasound and histomorphology in human coronary arteries. Heart 2001;85:567-70.

15. Komiyama N, Courtney BK, Toyozaki T, et al. In vivo on-line intravascular ultrasound radio-frequency signal analysis for tissue characterization of coronary atherosclerosis validated by histology of coronary atherectomy tissue specimens. Circulation 2001;104: II-590 [abstract].

16. Kawasaki M, Takatsu H, Noda T, et al. In vivo quantitative tissue characterization of human coronary arterial plaques by use of integrated backscatter intravascular ultrasound and comparison with angioscopic findings. Circulation 2002;105:2487-92.

17. Nair A, Kuban BD, Tuzcu EM, et al. Coronary plaque classification with intravascular ultrasound radiofrequency data analysis. Circulation 2002;106:2200-6.

18. Mintz GS, Nissen SE, Anderson WD, et al. ACC Clinical Expert Consensus Document on Standards for the acquisition, measurement and reporting of intravascular ultrasound studies: a report of the American College of Cardiology Task Force on Clinical Expert Consensus Documents (Committee to Develop a Clinical Expert Consensus Document on Standards for Acquisition, Measurement and Reporting of Intravascular Ultrasound Studies IVUS). J Am Coll Cardiol 2001;37:1478-92.

19. Fager G, Wiklund O. Cholesterol reduction and clinical benefit. Are there limits to expectations? Arterioscler Thromb Vasc Biol 1997;17: 3527-33.

20. Schartl M, Bocksch W, Koschyk DH, et al. Use of intravascular ultrasound to compare effects of different strategies of lipid-lowering therapy on plaque volume and composition in patients with coronary artery disease. Circulation 2001;104:387-92.

21. Pitt B, Waters D, Brown WV, et al. Aggressive lipid-lowering therapy compared with angioplasty in stable coronary artery disease. Atorvastatin versus Revascularization Treatment Investigators. N Engl J Med 1999;341:70-6.

22. Nissen SE, Tuzcu EM, Schoenhagen P, et al. Effect of intensive compared with moderate lipid-lowering therapy on progression of coronary atherosclerosis. A randomized controlled trial. JAMA 2004;291:1071-80.

23. Jensen LO, Thayssen P, Pedersen KE, et al. Regression of coronary atherosclerosis by simvastatin. A serial intravascular ultrasound study. Circulation 2004;110:265-70.

24. Okazaki S, Yokoyama T, Miyauchi K, et al. Volumetric intravascular ultrasound analysis during half a year after coronary event: the ESTABLISH study. Circulation 2004;110:1061-8.

25. Tearney GJ, Yabushita H, Houser SL, et al. Quantification of macrophage content in atherosclerotic plaques by optical coherence tomography. Circulation 2003;107:113-9.

26. Stefanadis C, Diamantopoulos L, Vlachopoulos C, et al. Thermal heterogeneity within human atherosclerotic coronary arteries detected in vivo. A new method of detection by application of a special thermography catheter. Circulation 1999;99:1965-71.

Infertility with Defective Spermiogenesis in Mice Lacking AF5q31, the Target of Chromosomal Translocation in Human Infant Leukemia

Atsushi Urano,[1,2] Masaki Endoh,[3] Tadashi Wada,[3] Yoshihiro Morikawa,[4] Miyuki Itoh,[2] Yuki Kataoka,[5] Tomohiko Taki,[6] Hiroshi Akazawa,[7] Hideaki Nakajima,[8] Issei Komuro,[7] Nobuaki Yoshida,[5] Yasuhide Hayashi,[9] Hiroshi Handa,[3] Toshio Kitamura,[2] and Tetsuya Nosaka[1]*

Division of Hematopoietic Factors,[1] Division of Cellular Therapy,[2] Laboratory of Gene Expression and Regulation, Center for Experimental Medicine,[5] and Center of Excellence,[8] Institute of Medical Science, University of Tokyo, Tokyo 108-8639, Graduate School of Bioscience and Biotechnology, Tokyo Institute of Technology, Midori-ku, Yokohama 226-8501,[3] Department of Anatomy and Neurobiology, Wakayama Medical University, Wakayama 641-8509,[4] Department of Molecular Laboratory Medicine, Kyoto Prefectural University of Medicine Graduate School of Medical Science, Kyoto 602-8566,[6] Department of Cardiovascular Science and Medicine, Graduate School of Medicine, Chiba University, Chiba 260-8670,[7] and Gunma Children's Medical Center, Gunma 377-8577,[9] Japan

AF5q31 (also called MCEF) was identified by its involvement in chromosomal translocation with the gene MLL (mixed lineage leukemia), which is associated with infant acute lymphoblastic leukemia. Several potential roles have been proposed for AF5q31 and other family genes, but the specific requirements of AF5q31 during development remain unclear. Here, we show that AF5q31 is essential for spermatogenesis. Although most AF5q31-deficient mice died in utero and neonatally with impaired embryonic development and shrunken alveoli, respectively, 13% of AF5q31-deficient mice thrived as wild-type mice did. However, the male mice were sterile with azoospermia. Histological examinations revealed the arrest of germ cell development at the stage of spermiogenesis, and virtually no spermatozoa were seen in the epididymis. AF5q31 was found to be preferentially expressed in Sertoli cells. Furthermore, mutant mice displayed severely impaired expression of protamine 1, protamine 2, and transition protein 2, which are indispensable to compact the haploid genome within the sperm head, and an increase of apoptotic cells in seminiferous tubules. Thus, AF5q31 seems to function as a transcriptional regulator in testicular somatic cells and is essential for male germ cell differentiation and survival. These results may have clinical implications in the understanding of human male infertility.

Chromosomal translocation is one of the common pathogenic mechanisms in various human malignancies, particularly in leukemias and lymphomas, and genes located at the breakpoints are involved in disease pathogenesis (21, 59, 60). The mixed lineage leukemia gene MLL (also called HRX, HTRX, and ALL-1) is frequently targeted by chromosomal rearrangements and is associated with clinically aggressive lymphoid and myeloid leukemias which are particularly prevalent in infant leukemias and treatment-related secondary leukemias (2, 18, 24, 64). MLL located on 11q23 is a human homologue of *Drosophila trithorax*, has a SET domain that normally functions as histone methyltransferase, and is assembled into a super-multiprotein complex with additional chromatin-remodeling components (45, 50, 70). Importantly, most of the leukemic variants of MLL lack the SET domain (7). In *Drosophila*, genetic evidence suggests that Trithorax controls the expression of *homeobox* (Hox) genes and regulates embryogenesis (39, 44, 47). In MLL-deficient mice, Hox gene expression initiates normally but is not maintained after 9.5 days postcoitus (dpc), demonstrating the importance of MLL in the mainte-

nance of Hox gene expression (72, 73). Hox genes also play an important role in hematopoietic differentiation, and their expression levels are upregulated in the human leukemias carrying MLL rearrangements (1). An unusual feature of MLL fusion proteins is the large number and diversity of heterologous proteins that fuse with MLL. To date, the MLL locus has been found to be translocated to approximately 40 different genetic loci and at least 30 of the partner genes have been characterized (13, 31). The functions of most MLL partner genes are unknown. Although no consistent homologies or common motifs that are characteristic to all the partner gene sequences have been identified, some are classified into small subgroups according to their sequence homologies. Of interest is that the fusion partner plays an important role in determining disease features.

The (5;11)(q31;q23) translocation is associated with infant acute lymphoblastic leukemia (ALL) (63). This translocation juxtaposes the 5' sequences of the MLL gene to the 3' sequences of the AF5q31 gene and results in the formation of an in-frame MLL-AF5q31 fusion protein which contains the amino-terminal region of MLL, including its AT hooks, methyltransferase domain, and repression domain, and amino acids 351 to 1163 of AF5q31, including the transactivation domain in part and C-terminal homology domain. Based on the significant homology to multiple regions of the predicted AF5q31

* Corresponding author. Mailing address: Institute of Medical Science Division of Hematopoietic Factors, University of Tokyo, 4-6-1 Shirokanedai, Minato-ku, Tokyo 108-8639, Japan. Phone: 81-3-5449-5399. Fax: 81-3-5449-5453. E-mail: tenosaka@ims.u-tokyo.ac.jp.

protein, three other mammalian *AF5q31* homology genes, *AF4*, *LAF4*, and *FMR2*, are known (2). Both *AF4* and *LAF4* have been independently identified as *MLL* partner genes in each case of pediatric ALL (19, 29, 46, 49, 65). In contrast, *FMR2* has not been observed in association with chromosome translocation in leukemia, but congenital mutations in the *FMR2* gene are involved in mild hereditary mental retardation (8, 22, 25). DNA binding and transcriptional properties of AF4, LAF4, and FMR2 suggest that *AF5q31* and other family genes function as nuclear transcription factors (28, 41, 53, 58). Recently, AF5q31 was found to interact with positive transcription elongation factor b (P-TEFb), which activates transcription by RNA polymerase II (RNAPII), leading to the formation of progressive elongation complex (20). Although transfection studies suggested that AF5q31 acts as a repressor of RNAPII transcription, the precise role of AF5q31 in the transcriptional activity of P-TEFb is not known.

AF4 knockout mice demonstrated that AF4 is required for normal lymphopoiesis (34). In the bone marrow of the mutant mice, loss of AF4 function did not disrupt progenitor B-cell development; however, the transition from pre-B cell to the newly generated mature B cell was severely reduced and exhibited defective thymocyte development from a double-negative to a double-positive population. These findings may provide insights into lymphoid leukemogenesis by MLL-AF4. On the other hand, robotic mice carrying autosomal dominant missense mutation in the *AF4* gene have been identified from a large-scale *N*-ethyl-*N*-nitrosurea (ENU) mutagenesis pool (32). As a result, newborn mice developed a severe loss of Purkinje cells of the cerebellum within several weeks after birth and showed a strange ataxic gait. But the thymic double-negative and double-positive populations were not significantly different in the mutant and control mice. Interestingly, AF4 interacts with the E3 ubiquitin ligase SIAH1 and the minimal interaction domain of AF4 to bind to SIAH1 was demonstrated to possess the PXAXVXP motif conserved within *AF5q31* and other family genes (6, 57). A missense mutation V294A in the robotic mice corresponds to Val of the PXAXVXP motif, and the Val mutation of the AF4 protein has been shown to reduce the binding ability to SIAH1 protein significantly, suggesting that the phenotype of the robotic mice is caused by an increased steady-state level of AF4 protein and that all the members of the AF5q31 family are regulated by this interaction (57). Since mutation of the *AF4* gene in the robotic mice occurred upstream of known translocation breakpoints, it is possible that MLL-AF4 may be more stable than AF4. However, the function of AF4 in the robotic mice would not directly account for the leukemogenic potential of MLL-AF4. Thus, there are few available data on the biological and pathological functions for *AF5q31* and other family genes.

We found that *AF5q31* is expressed during mouse embryogenesis at the highest level around 10.5 to 12.5 dpc and is widely expressed in adult mice, especially in Sertoli cells of the testis. This pattern suggests a specific role of AF5q31 during the differentiation of male germ cells. To gain insights into the potential role for AF5q31 in leukemogenesis and normal development, we disrupted the *AF5q31* gene by homologous recombination and examined the mutant phenotype of the mice. Here, we show that AF5q31 deficiency resulted in embryonic and neonatal lethality in most mice but that some survived to

grow properly except for azoospermia, thus raising the possibility that *AF5q31* mutations will be found in some patients with autosomal recessive azoospermia.

MATERIALS AND METHODS

Plasmids. To obtain the mouse *AF5q31* (m*AF5q31*) expression construct, the DNA sequence of full-length m*AF5q31* (GenBank accession number AF190449) was amplified by PCR from Ba/F3 cDNA and subcloned into pcDNA3.1 (Invitrogen) with a FLAG tag.

Antibodies. To prepare the anti-AF5q31 antibody that can recognize both human and mouse AF5q31 proteins, we prepared polyclonal antibodies against the highly conserved transactivation domain of mAF5q31 (E4; 317 to 492 amino acids). DNA sequences corresponding to this region were amplified by PCR and subcloned into pGEX-4T (Amersham Biosciences). Anti-mAF5q31 antisera were raised in rabbits against the purified GST-mAF5q31-E4 (317- to 492-amino acid) fusion protein, depleted of anti-glutathione *S*-transferase (GST) antibodies, and further affinity purified on an antigen column.

To detect RNAPII, N20 antibody that reacts with both the hyperphosphorylated (IIo) and hypophosphorylated (IIa) forms of RNAPII was purchased from Santa Cruz. H5 and H14 antibodies that recognize Ser2 and Ser5 of the carboxy-terminal domain (CTD) phosphopeptides of RNAPII, respectively, were obtained from Covance Co. (Berkeley, CA). In addition, anti-α-tubulin (T-5168; Sigma) was used.

Generation of AF5q31-deficient mice. A phage clone containing an approximately 17-kb DNA fragment was isolated from a mouse 129 SvJ λ genomic library (Stratagene) with the m*AF5q31* cDNA probe. The *AF5q31* targeting vector was constructed by replacing the 5.0-kb HaeII-SspI DNA fragment that contains exon II harboring the initiation codon and exon III with a 1.1-kb fragment of the neomycin-resistant gene (*neo*) cassette of pMC1NeoPolyA (Stratagene) in an antisense orientation. The 2.2-kb fragment of the herpes simplex virus thymidine kinase gene cassette was inserted upstream of the *AF5q31* gene in an antisense orientation for negative selection. The linearized targeting plasmid DNA was electroporated into E14-1 embryonic stem (ES) cells. After double selections with 600 μg/ml G418 (Invitrogen) and 2 μM ganciclovir (Sigma), resistant clones were screened for homologous recombination by Southern blot analysis as described previously (54, 55). In brief, genomic DNA was digested with HindIII, separated by agarose gel electrophoresis, and transferred to a Hybond-N+ membrane (Amersham Biosciences). Hybridization was carried out with a 0.3-kb 3′ flanking probe. The targeting frequency was 12/384. ES cells from each of four independent *AF5q31* mutant clones were injected into C57BL/6 blastocysts. The blastocysts were transferred to pseudopregnant ICR foster mothers, and chimeras derived from two independent clones transmitted the mutant allele through their germ line. All animal experiments were done according to the guidelines for animal use issued by the Committee of Animal Experiments, Institute of Medical Science, University of Tokyo.

The genotype was also determined by PCR with Ex Taq (TaKaRa, Otsu, Japan). Genomic DNAs were prepared from mouse tail snips. For the wild-type and mutant alleles of the *AF5q31* gene, an antisense primer specific for the wild-type (5′-GTCTTCACGGTTCATGTTGC-3′) or mutant allele (5′-GCCCG GTTCTTTTTGTCAAG-3′, a sequence in the *neo* gene) was used with a common sense primer (5′-GTGGGTTATGTGCCACCAAA-3′). PCR was done at 96°C for 5 min for initial denaturing, followed by 35 cycles at 96°C for 1 min, 56°C for 1 min, and 72°C for 2 min.

Histology and immunohistochemistry. Formalin-fixed, paraffin-embedded sections (6 μm in thickness) of embryos were stained with hematoxylin and eosin stain. Bouin-fixed, paraffin-embedded sections of testes and epidydimides were stained with hematoxylin and eosin stain. For immunohistochemistry, formalin-fixed, paraffin-embedded sections (6 μm) of testes were deparaffinized, rehydrated, quenched of endogenous peroxidase activity with 3% hydrogen peroxide, and incubated overnight at 4°C with an anti-mAF5q31-E4 antibody. After washing of the sections three times in phosphate-buffered saline, samples were incubated with anti-rabbit immunoglobulin ENVISION horseradish peroxidase (DakoCytomation). The sections were counterstained with hematoxylin.

Northern blot analysis and PCR with reverse transcription (RT-PCR). Mouse multiple tissue blot (Clontech) was hybridized with the ³²P-labeled m*AF5q31* full-length cDNA probe followed by rehybridization with a mouse *AF4*, *LAF4*, and *FMR2* probe and a human glyceraldehyde-3-phosphate dehydrogenase (GAPDH) cDNA probe, as described previously (55, 56). Mouse embryo full-stage blot (Seegene) was hybridized with the m*AF5q31* cDNA probe. The mouse *AF4* and *LAF4* cDNA probes were obtained by PCR amplification from a mouse

thymus cDNA library and the mouse *FMR2* cDNA probe from a mouse brain cDNA library. The human GAPDH cDNA probe was described previously (56). The following oligonucleotide primers specific to mouse *AF4*, *LAF4*, and *FMR2* were used: for *AF4*, 5'-CCTGCTTCGAATCAGAGAGA-3' (sense) and 5'-CA TCCTTAGTCTGGTGAGCT-3' (antisense); for *LAF4*, 5'-GGAGGAAAGAG CGAGAAAGA-3' (sense) and 5'-CCCTCTCCATATTGCACACT-3' (antisense); and for *FMR2*, 5'-GCAGTGTCACTATGAACAAG-3' (sense) and 5'-CCAGGTGCTTGCACTGTAAA-3' (antisense).

To confirm the gene disruption of m*AF5q31*, total RNAs from mouse embryonic fibroblasts (MEFs) obtained derived from 13.5-dpc embryos and maintained in Dulbecco's modified Eagle medium containing 10% fetal bovine serum were isolated with Trizol reagent (Invitrogen). Total RNA (3 μg) was reverse transcribed using Superscript reverse transcriptase II (Invitrogen) with random primers in a total volume of 20 μl. One μl of this reaction mixture was used as a template for PCR amplification with Ex Taq (TaKaRa) in the following condition: at 96°C for 5 min for initial denaturing, followed by 35 cycles at 96°C for 30 s, 56°C for 30 s, and 72°C for 1.5 min. The following oligonucleotide primers specific to m*AF5q31* exons I to IV and GAPDH for a control were used: for *AF5q31* exons I to IV, 5'-GAAATGGTTCGGGCCTAGCG-3' (sense) and 5'-CTACACAGCTTACATCACCA-3' (antisense), and for GAPDH, 5'-ACCAC AGTCCATGCCATCAC-3' (sense) and 5'-TCCACCACCCTGTTGCTGTA-3' (antisense).

To assess the expression levels of several genes in testis, RT-PCR analyses were performed on total RNAs derived from the testes of 12-week-old AF5q31^{+/+}, AF5q31^{+/−}, and AF5q31^{−/−} male mice and 9-week-old WBB6F1-W/W[v] male mice (Japan SLC) using the same methods as in MEFs. The following oligonucleotide primers specific for *TP1*, *TP2*, *Prm1*, *Prm2*, *Tpap*, *RT7*, *Hsc70t*, *Mcs*, *Pgk2*, *Camk4*, *CREM*, *TRF2*, *RARα*, *RXRβ*, *AR*, *FSH-R*, *LH-R*, and *GATA1* were used: for *TP1*, 5'-ATGTCGACCAGCCGCAAGCT-3' (sense) and 5'-TCACAAGTGGGATCGGTAAT-3' (antisense); for *TP2*, 5'-GCCTCAAAG TCACACCAGTA-3' (sense) and 5'-ACTTGTATCTTCGCCCTGAG-3' (antisense); for *Prm1*, 5'-ATGCTGCCGCAGCAAAAGCA-3' (sense) and 5'-CAC CTTATGGTGTATGAGCG-3' (antisense); for *Prm2*, 5'-ATGGTTCGCTACC GAATGAG-3' (sense) and 5'-TTAGTGATGGTGCCTCCTAC-3' (antisense); for *Tpap*, 5'-GGCTCTTACCGATTAGGAGT-3' (sense) and 5'-AGTTACCC GGCAACCGTTAA-3' (antisense); for *RT7*, 5'-TGCCTGTGTGACTACAAG CT-3' (sense) and 5'-AGTACGTCACGTCCTTCTCA-3' (antisense); for *Hsc70t*, 5'-CCATGAATCCCCAGAACACT-3' (sense) and 5'-ATGACACCTG CATCCTTGGT-3' (antisense); for *Mcs*, 5'-ACCATGTTGCCCACCTAAAC-3' (sense) and 5'-TCTCCAGAGTTTGGCCAGAT-3' (antisense); for *Pgk2*, 5'-C TGTTGCTGATGAGCTCAAG-3' (sense) and 5'-ACTCCGACCATAGAACT GTG-3' (antisense); for *Camk4*, 5'-TCTCTCACACCCGAACATCA-3' (sense) and 5'-GGTTCCACACACTGTCTTCA-3' (antisense); for *CREM*, 5'-ACTTT CCTCTGATGTGCCTG-3' (sense) and 5'-CTTGCGAGTTGCTTCTTCTG-3' (antisense); for *TRF2*, 5'-TGCTTTGGAGGGAGCAAATG-3' (sense) and 5'-AGTTCAGGTTCATAGCTGGC-3' (antisense); for *RARα*, 5'-TTGAGAAGG TTCGCAAAGCG-3' (sense) and 5'-AGGTCAGTGTGTCTTGCTCA-3' (antisense); for *RXRβ*, 5'-AGACTGTACAGTGGACAAGC-3' (sense) and 5'-TG GCAGATGTTAGTCACTGG-3' (antisense); for *AR*, 5'-ACCCTATCCCAGT CCCAATT-3' (sense) and 5'-GATGGGCAATTTTTCCTCCG-3' (antisense); for *FSH-R*, 5'-CGGAACGCCATTGAACTGAG-3' (sense) and 5'-CAAAGCT CAGTCCCATGAAG-3' (antisense); for *LH-R*, 5'-TGCACTCTCCAGAGTTG TCA-3' (sense) and 5'-TCTTCGAAACATCTGGGAGG-3' (antisense); and for *GATA1*, 5'-CAGGTTTCTTTTCCTCTGGG-3' (sense) and 5'-AAAGGACTG GGAAAGTCAGC-3' (antisense).

To monitor the expression of *AF5q31* in the juvenile mice testes at various stages, RT-PCR analyses were done on total RNAs derived from C57BL/6 male mice (Japan SLC) at various ages, using the same methods as in MEFs. The sequence within the *AF5q31* exons V to VIII was amplified with the primers 5'-CGGCTATTCATACACCATGC-3' (sense) and 5'-CTCCCTCACTGTTAT GGTGT-3' (antisense).

Terminal deoxynucleotidyltransferase-mediated dUTP nick end labeling (TUNEL) assay. Formalin-fixed, paraffin-embedded testis sections (6 μm) of 12-week-old mice were prepared, and apoptotic cells were detected in situ using ApoAlert DNA fragmentation assay kits (Clontech). The cells were counterstained with 4',6-diamidino-2-phenylindole [DAPI].

Western blot analysis. An equal amount of total cell lysates from MEFs (10 μg/lane) was separated in 4 to 20% gradient polyacrylamide gels. Proteins were transferred onto a nitrocellulose membrane. The blot was incubated with the primary antibody at room temperature for 1 h and with a horseradish peroxidase-conjugated secondary antibody at room temperature for 1 h. Enhanced chemiluminescence Western blotting detection reagents (Amersham Biosciences) were used for detection.

Assessment of serum hormone levels. The blood of male AF5q31^{+/+}, AF5q31^{+/−}, and AF5q31^{−/−} mice (<24 weeks) was drawn by cardiocenthesis and stored on ice for 30 min. After 10 min of centrifugation at 800 × *g* for 10 min, the serum was collected and stored at −80°C until analysis. The levels of serum testosterone, luteinizing hormone (LH), and follicle-stimulating hormone (FSH) were measured by SRL Co. (Tokyo, Japan).

Fertility assessment. The reproductive capacities of 9-week-old male AF5q31^{+/+}, AF5q31^{+/−}, and AF5q31^{−/−} mice were investigated by mating one male with two 8-week-old C57BL/6j females for 2 weeks, as described previously (10, 26). Female mice were checked for vaginal plugs each morning, and litter sizes were recorded on delivery after three successive matings.

Evaluation of epididymal sperm. The cauda epididymides were removed and minced in 0.1 ml of motile buffer (120 mM NaCl, 5 mM KCl, 25 mM NaHCO$_3$, 1.2 mM KH$_2$PO$_4$, 1.2 mM MgSO$_4$, 1.3 mM CaCl$_2$). The tissues were incubated at 37°C for 5 min to allow sperm to disperse, as described previously (48).

Generation and purification of the recombinant proteins. Human *AF5q31* cDNA (63) was subcloned into pBacPAK8 vector (BD Biosciences) with a hemagglutinin (HA) tag on the N terminus and a FLAG tag on the C terminus. AF5q31 was expressed in Sf9 cells by using a BacPAK baculovirus expression kit (BD Biosciences) according to the manufacturer's instructions. Sf9 cells were solubilized in lysis buffer (50 mM Tris-Cl [pH 7.5], 150 mM NaCl, 1 mM EDTA, 1.0% Triton X-100) supplemented with protease inhibitor cocktails (Sigma). The extract was loaded onto an anti-FLAG M2 agarose (Sigma) column equilibrated with TBS buffer (50 mM Tris-Cl [pH 7.5], 150 mM NaCl), and bound proteins were eluted with TBS buffer supplemented with 0.2 mg/ml FLAG peptide (Sigma). Proteins in the elution were loaded onto an anti-HA 3F10 affinity matrix (Roche) column equilibrated with TBS buffer containing 0.1% NP-40, and bound proteins were eluted with HGKEN buffer (20 mM HEPES-NaOH [pH 7.9], 20% glycerol, 100 mM KCl, 0.2 mM EDTA, 0.1% NP-40) supplemented with 1 mg/ml HA peptide (Roche). Proteins in the eluate were further separated on a Mono Q column (Amersham Biosciences) equilibrated with HGKEN buffer containing 5 mM β-mercaptoethanol and 0.5 mM phenylmethylsulfonyl fluoride by elution with a linear gradient from 200 mM to 400 mM KCl. Each fraction was dialyzed against HGKEN buffer containing 1 mM dithiothreitol and 1 mM phenylmethylsulfonyl fluoride. GST-CTD and P-TEFb were purified as described previously (66, 67).

CTD kinase assay. GST-CTD was incubated with purified P-TEFb and each recombinant AF5q31 fraction in the presence of 60 μM ATP containing [γ-^{32}P]ATP in transcription buffer for 10 min at 30°C as described previously (66, 67). Reaction products were subjected to 4 to 20% gradient polyacrylamide gel electrophoresis followed by autoradiography.
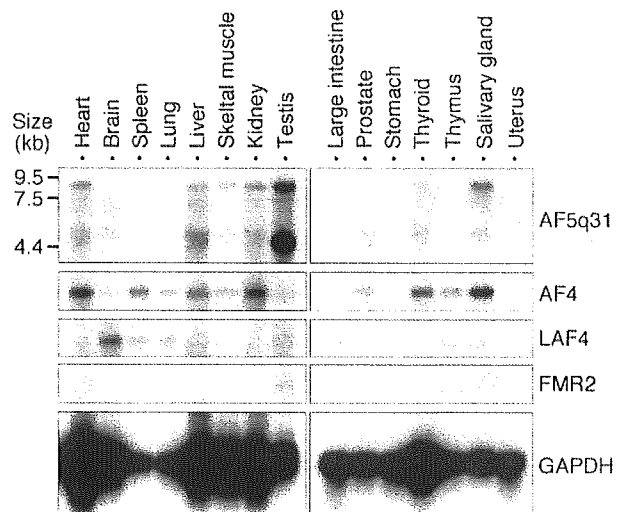

FIG. 1. Expression profiles of mouse *AF5q31* and *AF5q31* family genes in adult normal tissues. Northern blot analysis of poly(A) RNAs (2 μg/lane) from normal mouse tissues. The blot was hybridized to radioactive mouse *AF5q31*, *AF4*, *LAF4*, and *FMR2* probes. As a control, the same blot was rehybridized with a GAPDH probe.
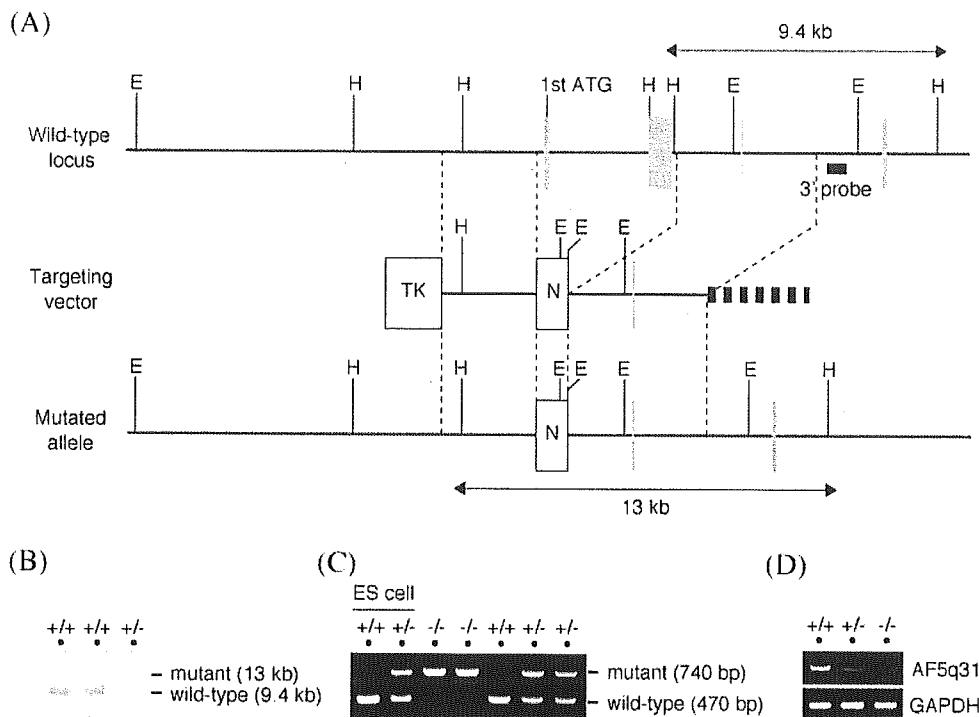
FIG. 2. Targeted disruption of the *AF5q31* gene. (A) Schematic representation of the wild-type allele of mouse *AF5q31* (top), the targeting vector (middle), and the mutant allele resulting from a homologous recombination (bottom). Filled boxes are exons, and open boxes are selection marker genes. H, HindIII restriction site; E, EcoRI restriction site; N, neomycin resistance gene cassette; TK, thymidine kinase gene cassette. (B) Southern blot analysis of HindIII-digested genomic DNAs (5 µg/lane) from ES clones with an external 3′ probe. The 9.4-kb and 13-kb bands represent the wild-type and targeted alleles, respectively. An external 3′ probe used to analyze is shown in panel A. (C) PCR-based genotype analysis of tail DNAs isolated from the pups of AF5q31$^{+/-}$ intercrosses. Three kinds of primers (see Materials and Methods) detected both the wild-type allele (470-bp band) and the targeted allele (740-bp band). As controls, parental and targeted ES cells were used. (D) RT-PCR analysis of total RNAs from AF5q31$^{+/+}$, AF5q31$^{+/-}$, and AF5q31$^{-/-}$ MEFs. The primers located on exons I and IV of the *AF5q31* gene were used. RT-PCR for GAPDH confirms equivalent amounts of RNAs used for the analysis.

RESULTS

High expression of *AF5q31* in testis. To explore the tissue distribution of *AF5q31*, Northern blot analysis was performed on various tissues of the adult mice. *AF5q31* was present at a high level in testis and low levels in several other tissues (Fig. 1). Rehybridizations were also carried out with *AF4*, *LAF4*, and *FMR2* cDNA probes. Expression of *AF4* was detected in the heart, kidney, thyroid, and salivary gland at relatively high levels and at low levels in the spleen, liver, and thymus, as reported elsewhere (4). *LAF4* transcript was expressed in the brain and weakly in the spleen and lung. Previously, mouse *LAF4* was shown to be expressed predominantly in the thymus and the spleen of adult mice (41); however, we could not reproduce these results. Almost no signal of *FMR2* expression, except in the testis, was consistent with the finding in the previous report that the expression of *FMR2* occurs on or around 7.0 dpc, reaches its highest level at 10.5 to 11.5 dpc, and is very slight in other stages (9). Compared with these expression profiles, *AF5q31* transcript in the testis was remarkably high.

Targeted disruption of *AF5q31*. To clarify the physiological role of AF5q31, AF5q31$^{-/-}$ mice were generated by gene targeting. Examination of the sequences in the databases revealed that the mouse *AF5q31* gene consists of at least 21 exons (coding exons II to XXI) within 70 kb of the genomic

DNA. The region encoded by exons II and III carries the N-terminal homology domain and the partial transactivation domain conserved in AF5q31, AF4, LAF4, and FMR2, which consists of the N-terminal 25% of AF5q31 (2). A targeting vector was constructed by replacing exons II and III with the *neo* gene (Fig. 2A) and introduced into mouse ES cells. ES clones carrying the mutation were identified using Southern blots and an external 3′ probe (Fig. 2B). The blot rehybridized with a *neo* probe yielded only the 13-kbp band, and the EcoRI-digested genomic DNAs probed with an external 5′ probe

TABLE 1. Genotyping of staged embryos and newborn pups by AF5q31$^{+/-}$ intercrossing

Embryonic stage	No. of embryos				
	Progeny with the following genotypes:			Resorbed	Total
	+/+	+/-	-/-		
8.5 dpc	14	11	9 (1^a)		34
9.5 dpc	4 (1^a)	9	10		23
10.5 dpc	9 (1^a)	14 (1^a)	8 (4^a)	1	32
12.5 dpc	7	11	3	11	32
Newborn	44 (6^b)	115 (6^b)	24 (17^b)		183

^{a} Number of growth-retarded embryos.
^{b} Number of neonates dead within 24 h of birth.

(A)   (B)   (C)

(D)   (E)

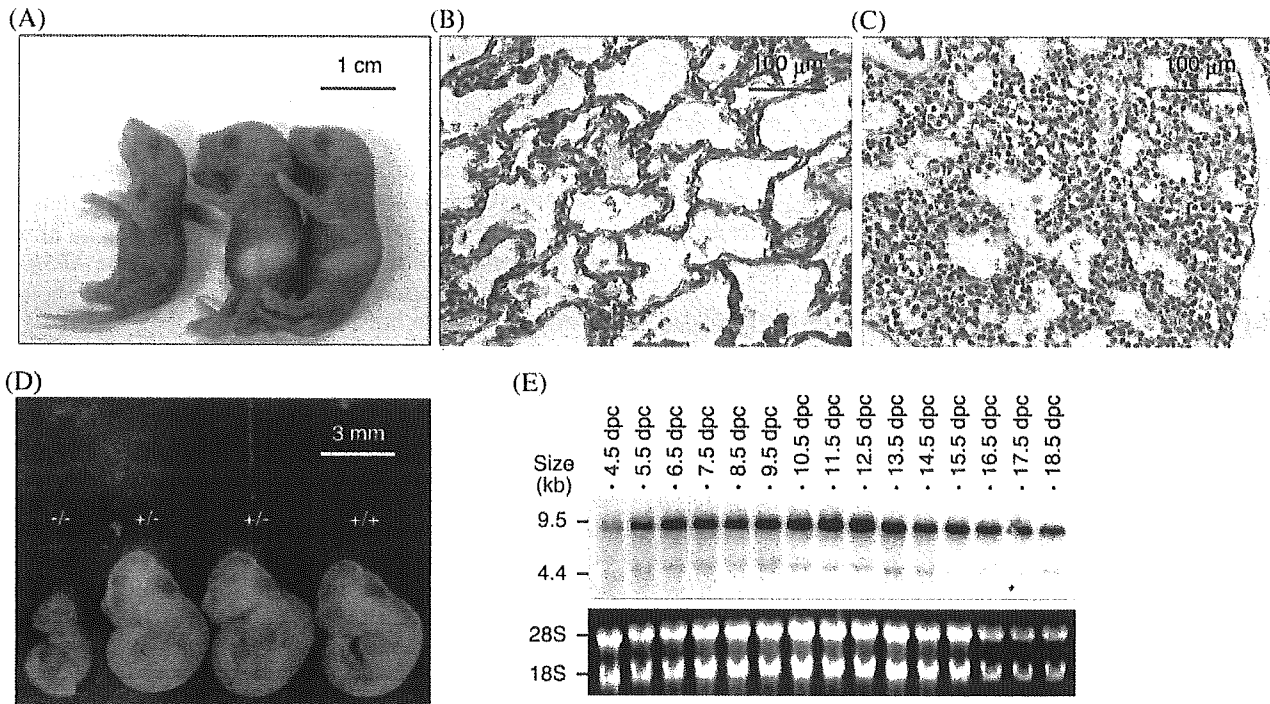FIG. 3. Macroscopic and microscopic analyses of AF5q31-deficient mice at different ages and the expression profiles of *AF5q31* in the normal mouse embryos. (A) Gross morphology of neonatal littermates representing AF5q31$^{+/+}$ (right), AF5q31$^{+/-}$ (center), and AF5q31$^{-/-}$ (left). (B and C) Histological sections of the lung from AF5q31$^{+/+}$ (B) and AF5q31$^{-/-}$ (C) neonatal littermates stained with hematoxylin and eosin stain. (D) Gross morphology of the AF5q31$^{+/+}$, AF5q31$^{+/-}$, and AF5q31$^{-/-}$ embryos of a litter at 10.5 dpc. (E) Northern blot analysis of total RNAs (20 µg/lane) from each embryo stage of the wild-type mouse. The blot was hybridized to a radioactive *AF5q31* probe. As a loading control, 18S and 28S rRNAs in total RNA are demonstrated.

further corroborated appropriate homologous recombination (a 21-kbp band in the wild type and a 15-kbp band in the mutant) (data not shown). After injection of the ES clones into blastocysts, generation of the chimeric mice, and backcrossing of the chimeras, AF5q31$^{+/-}$ mice were obtained. Genotyping of the progenies from intercrosses of the heterozygotes by PCR revealed the presence of AF5q31$^{-/-}$ mice (Fig. 2C). To confirm the deletion in the *AF5q31* mRNA of the mutant mice, RNAs from the MEFs in AF5q31$^{+/+}$, AF5q31$^{+/-}$, and AF5q31$^{-/-}$ mice were analyzed by RT-PCR. When sequences from exons I and IV were used as primers, RT-PCR with RNAs from the AF5q31$^{+/+}$ and AF5q31$^{+/-}$ MEFs produced a band of 973 bp, whereas no bands were detected with RNA from the AF5q31$^{-/-}$ MEFs (Fig. 2D). This result indicated that the *AF5q31* mRNA in the mutant mice lacked the sequence for exons II and III.

AF5q31 is important for embryonic development. Genotype analysis of the neonates showed a decrease by 55% in the AF5q31$^{-/-}$ mice relative to the numbers of wild-type and heterozygous littermates, based on the Mendelian ratio, and 71% of the AF5q31$^{-/-}$ neonates died as early as 12 to 24 h postpartum (Table 1). It was noteworthy that neonates that would die had no milk spots and breathed abnormally (Fig. 3A). Precise histochemical analyses of the entire set of neonates revealed that the lethality of AF5q31$^{-/-}$ neonates was potentially caused at least in part by severely shrunken alveoli of the lung (Fig. 3C), compared with the lungs of wild-type mice (Fig. 3B).

When analyzed during gestation, AF5q31$^{-/-}$ mice accounted for 25% of all embryos at 10.5 dpc, demonstrating that disruption of the *AF5q31* gene does not affect the viability of embryos until this stage (Table 1). However, growth retardations, but no obvious malformations, were macroscopically observed in 50% of the mutant embryos at 10.5 dpc (Fig. 3D), and these embryos were likely to be absorbed at 12.5 dpc, indicating that up to 50% of the mutant embryos were lethal around these periods. The expression pattern during mouse development was examined to identify the correct time at which *AF5q31* expression occurs. Northern blot analysis on the RNAs from 4.5-dpc to 18.5-dpc mouse embryos revealed sustained expression of *AF5q31* throughout embryogenesis, and the expression reached its highest level at 10.5 to 12.5 dpc (Fig. 3E). Hence, *AF5q31* appears to be important for embryonic development in this period.

Failure of spermatogenesis in AF5q31$^{-/-}$ male mice. AF5q31$^{-/-}$ male and female mice that survived for >2 months (13% of the AF5q31$^{-/-}$ mice of the C57BL/6/129 background and none of the inbred 129 background so far) seemed normal in health and behavior, and no abnormalities in any organ or tissue examined were found (data not shown), except for the testis (see below). Interestingly AF5q31$^{-/-}$ males were infertile whereas AF5q31$^{-/-}$ females were fertile. Essentially, identical results were obtained in both mouse lines derived from two independent ES cell clones. AF5q31$^{+/-}$ male mice exhibited normal fertility. To evaluate fertility in 9-week-old AF5q31 mutant male mice, each of the AF5q31$^{+/+}$, AF5q31$^{+/-}$, and

TABLE 2. Fertility assessment

Mice	Avg. no. of litters			Vaginal plug[a]
	1	2	3	
AF5q31$^{+/+}$	10 ± 0	6.5 ± 0.5	8.5 ± 0.5	+
AF5q31$^{+/-}$	9 ± 1.0	7.5 ± 0.5	7 ± 0	+
AF5q31$^{-/-}$	0	0	0	±

[a] +, always gave vaginal plugs; ±, some gave vaginal plugs and some did not.

AF5q31$^{-/-}$ mice was mated with 8-week-old C57BL/6 female mice (10, 26). Although AF5q31$^{+/+}$ and AF5q31$^{+/-}$ male mice always gave vaginal plugs the morning after mating and impregnated their mates, some of the AF5q31$^{-/-}$ males failed to give vaginal plugs and all of the AF5q31$^{-/-}$ males could not impregnate their mates in three successive sets of 2-week pairings (Table 2). As a control, the same female mice (after 2 weeks of matings with AF5q31$^{-/-}$ male mice) were always impregnated after mating with C57BL/6 male mice.

Phenotype analysis showed that there was no detectable difference in the morphology of urogenital tracts between the wild-type and mutant mice (data not shown), albeit the sizes of the testes and epididymides in AF5q31$^{-/-}$ mice were significantly smaller and the body weights and the sizes of seminal vesicles were larger than those of AF5q31$^{+/+}$ and AF5q31$^{+/-}$ mice (Fig. 4A to E). Serum hormone assays showed that the

levels of testosterone, LH, and FSH in AF5q31$^{-/-}$ mice were not significantly different from those in AF5q31$^{+/+}$ mice in statistical analyses (Fig. 4F to H). Also, mRNAs for the androgen receptor (AR), LH-R, and FSH-R were equally expressed in the testes of AF5q31$^{-/-}$ and control littermates (see Fig. 6D). Consistent with the finding that AF5q31$^{-/-}$ mice were infertile, their seminal fluids were devoid of mature spermatozoa and only debris was present, indicating an arrest of spermatogenesis (Fig. 4I). The spermatozoa of the AF5q31$^{+/-}$ males displayed normal motility with no evident morphological abnormalities (data not shown).

To verify the defect in the spermatogenesis of AF5q31$^{-/-}$ mice, testes were histologically analyzed. As expected, no sperm were found in the cauda epididymides of the AF5q31$^{-/-}$ mice, in contrast to those of the wild-type mice, which accounts for the infertility of the mutant mice (Fig. 5A and B). Detailed histological analysis revealed that round spermatids in the seminiferous tubules of the AF5q31$^{-/-}$ mice differentiated until at least step 11 but failed to undergo normal morphological change to elongated spermatids and to be released as spermatozoa within the germinal epithelium, while somatic Sertoli cells appeared morphologically normal (Fig. 5D, F, and H) and the morphology of seminiferous tubules in the mutant mice was indistinguishable from that of the wild-type mice. In contrast, most stages of the spermatogenic cycles in wild-type mice were represented (Fig. 5C, E, and G). Thus,
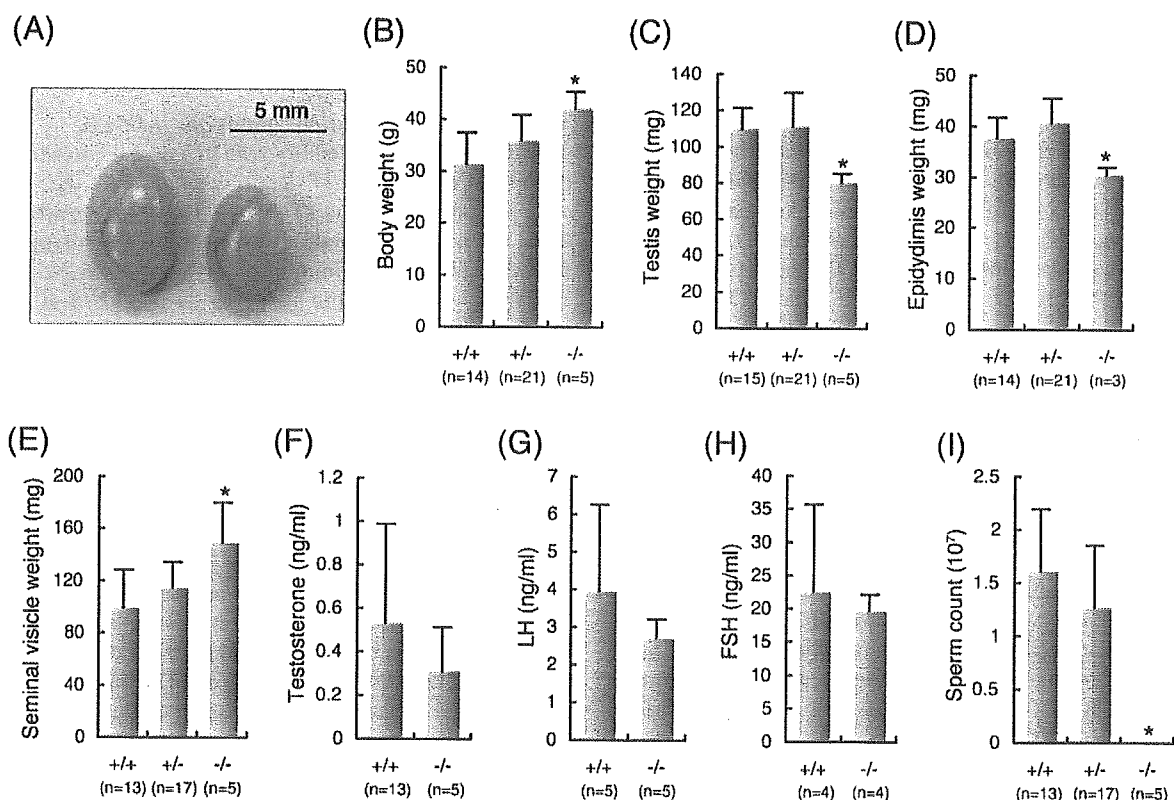

FIG. 4. Weights, hormone levels, and sperm counts in AF5q31$^{-/-}$ and control mice. (A) Testes from 24-week-old AF5q31$^{+/+}$ (left) and AF5q31$^{-/-}$ (right) male mice. (B to E) Weights of body and urogenital tracts of 12-week-old AF5q31$^{+/+}$, AF5q31$^{+/-}$, and AF5q31$^{-/-}$ male mice. (F to H) Serum testosterone, LH, and FSH levels in AF5q31$^{+/+}$ and AF5q31$^{-/-}$ male mice. (I) Numbers of sperm cells prepared from 12-week-old AF5q31$^{+/+}$, AF5q31$^{+/-}$, and AF5q31$^{-/-}$ male mice. The data are given as averages. Error bars represent standard errors. Statistical significance (∗, $P < 0.01$) in each assay was assessed using Student's t test between the wild-type and AF5q31$^{-/-}$ mice.
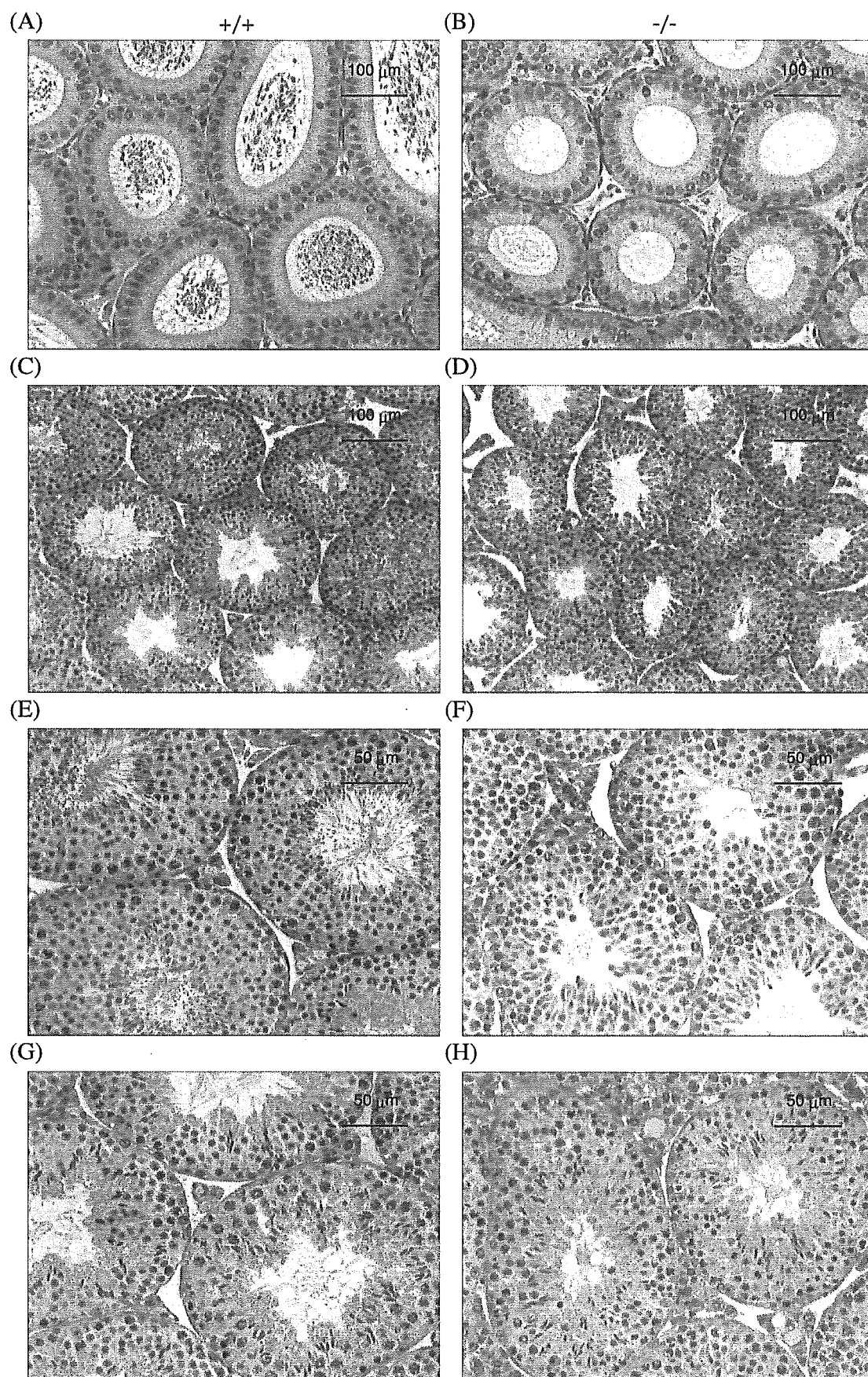
FIG. 5. Histology of epididymides and seminiferous tubules of AF5q31$^{+/+}$ and AF5q31$^{-/-}$ male mice. The epididymal (A and B) and testicular (C to H) sections from 24-week-old AF5q31$^{+/+}$ (A, C, E, and G) and AF5q31$^{-/-}$ (B, D, F, and H) male mice were stained with hematoxylin and eosin stain.

6840

-73-

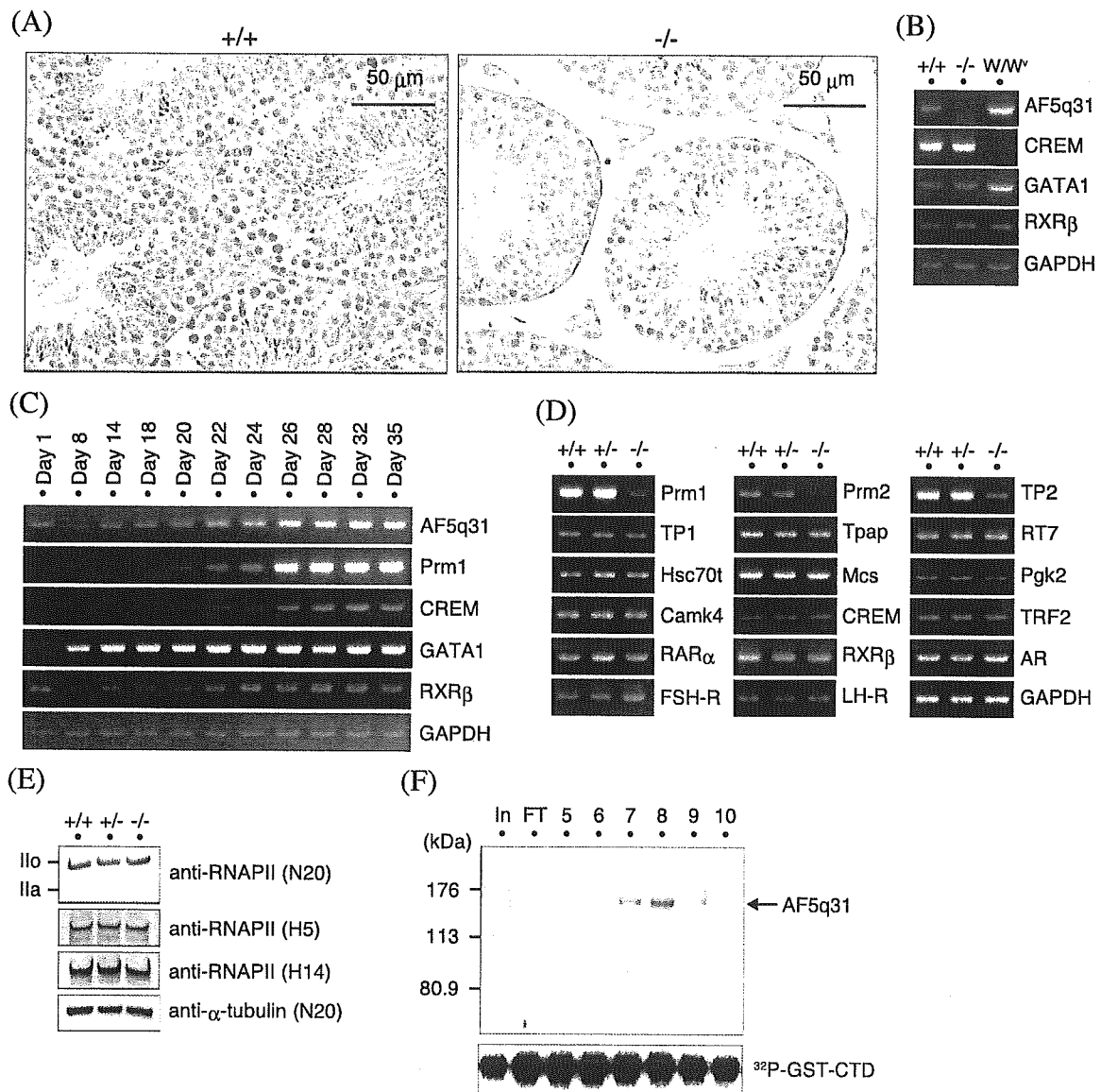FIG. 6. Mechanism of defective spermatogenesis in AF5q31-deficient mice. (A) Expression of AF5q31 in testes. Immunohistochemical staining was performed with an anti-mAF5q31-E4 antibody on sections of the testes of 12-week-old AF5q31$^{+/+}$ and AF5q31$^{-/-}$ mice. Sections were counterstained with hematoxylin. Brown areas represent the positive signals. (B) RT-PCR analyses of *AF5q31* expression using total RNAs isolated from the testes of 12-week-old AF5q31$^{+/+}$ and AF5q31$^{-/-}$ male mice and 9-week-old W/W^v male mice. RT-PCR for GAPDH confirms the equivalent amounts of RNAs used for the analysis. (C) Expression of *AF5q31* during juvenile testis development in mice. RT-PCR analyses of *AF5q31* exons V to VIII and several marker genes in testis are demonstrated. RT-PCR for GAPDH confirms the equivalent amounts of RNAs used for the analysis. (D) Expression of spermatogenesis- and spermiogenesis-related genes in the testes of 12-week-old AF5q31$^{+/+}$, AF5q31$^{+/-}$, and AF5q31$^{-/-}$ male mice. RT-PCR for GAPDH confirms the equivalent amounts of RNAs used for the analysis. (E) RNAPII CTD phosphorylation in AF5q31$^{+/+}$, AF5q31$^{+/-}$, and AF5q31$^{-/-}$ MEFs. Whole-cell extracts (10 μg/lane) were immunoblotted with the indicated antibodies. As a control, anti-α-tubulin was used to monitor the loading amounts. (F) In vitro kinase assay of P-TEFb in the presence or absence of AF5q31. Chromatography of purified HA-AF5q31-Flag on a Mono Q column revealed the presence of full-length AF5q31 (140 kDa). Each fraction (4 μl) on the Mono Q column was analyzed by SDS-PAGE and silver staining (upper panel). The lane marked "In" represents a part of the material before loading the column, and the lane marked "FT" indicates the flowthrough of the Mono Q column. Equal aliquots from each fraction were added to the kinase reaction mixture containing P-TEFb and GST-CTD and resolved by SDS-PAGE. Phosphorylated GST-CTD was detected by autoradiography (lower panel).

spermatogenesis is arrested at the stage of spermiogenesis in AF5q31$^{-/-}$ mice.

Mechanism of infertility in AF5q31$^{-/-}$ mice. Immunohistochemical analysis on testes with a purified anti-AF5q31 antibody disclosed that AF5q31 was expressed preferentially in Sertoli cells, weakly in germ cells, and barely in Leydig cells (Fig. 6A). Consistent with this finding is that *AF5q31* expression in RT-PCR analysis was elevated in c-*kit* mutant W/W^v male mice which harbor greatly reduced numbers of germ cells (38), compared with that in the mice with the normal c-*kit* gene (Fig. 6B). This pattern in RT-PCR analysis is similar to that of *GATA1* which is expressed only in Sertoli cells in the testis (71)
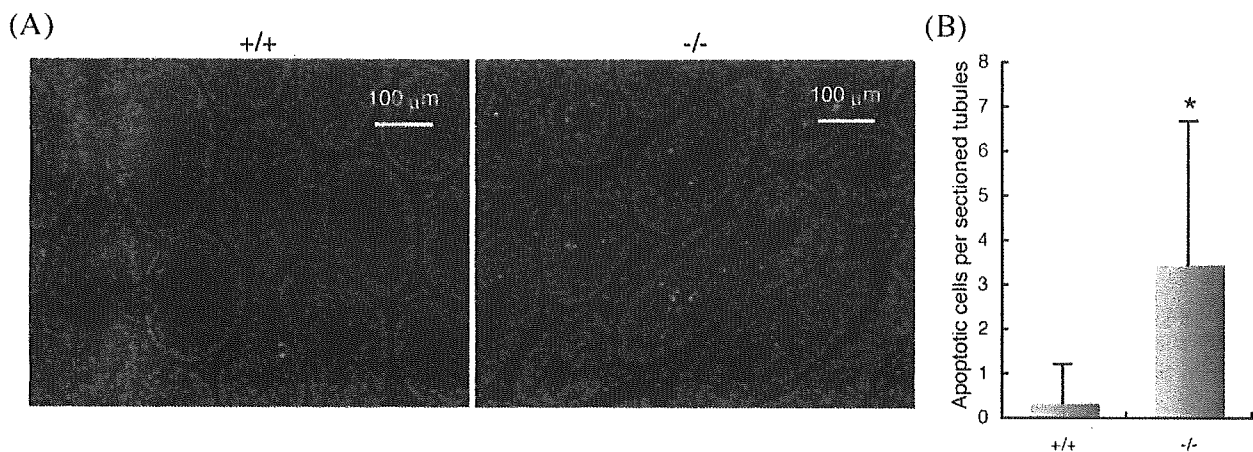
FIG. 7. Germ cell apoptosis in AF5q31$^{+/+}$ and AF5q31$^{-/-}$ mice. (A) Apoptotic cells detected by an in situ TUNEL assay in testis sections from 12-week-old AF5q31$^{+/+}$ (left) and AF5q31$^{-/-}$ (right) mice. TUNEL-positive cells were seen with fluorescein isothiocyanate (green). All the cells were visualized with DAPI (blue). (B) Quantification of apoptotic germ cells in the seminiferous tubules of 12-week-old AF5q31$^{+/+}$ and AF5q31$^{-/-}$ mice. In each testis, TUNEL-positive (apoptotic) nuclei in more than 100 randomly sectioned seminiferous tubules were counted and averaged. Error bars represent standard errors. Statistical significance (*, $P < 0.01$) was assessed by Student's t test.

and is the opposite of that of the cyclic AMP-responsive element modulator (CREM), which is exclusively expressed in postmeiotic germ cells in the testis (5, 51) (Fig. 6B). Furthermore, early expression of AF5q31 during testis development also supports the preferential expression of AF5q31 in Sertoli cells (Fig. 6C). As Sertoli cells are known to regulate spermatogenesis through the interactions with germ cells (23, 62), we determined if the transcription of some of spermatogenesis-related genes would be deregulated in AF5q31$^{-/-}$ mice by RT-PCR assays (Fig. 6D). Four genes which have critical roles in transcriptional regulation, CREM, TBP-related factor 2 (TRF2), retinoic acid receptor α (RARα), and retinoid X receptor β (RXRβ), were normally expressed in the testes of AF5q31$^{-/-}$ mice (5, 36, 40, 43, 51, 74). Furthermore, testis-specific cytoplasmic poly(A) polymerase (Tpap), sperm outer dense fiber protein (RT7), heat shock protein Hsc70t, mitochondria capsule selenoprotein (Mcs), and phosphoglycerate kinase-2 (Pgk2), which are known to be expressed in spermiogenesis, were not significantly changed, except for a slight decrease of Mcs in the mutant testes (35). After meiosis, histones are replaced by protamines (protamines 1 and 2 [Prm1 and Prm2, respectively]) through transition proteins (transition proteins 1 and 2 [TP1 and TP2, respectively]) in order to package the haploid genome within the sperm head in mammals (61). Intriguingly, expression levels of TP2, Prm1, and Prm2 were drastically decreased and that of TP1 was slightly decreased in AF5q31$^{-/-}$ testes. But the expression levels of Ca^{2+}/calmodulin-dependent protein kinase IV (Camk4), which is expressed in spermatids and phosphorylates Prm2, did not differ among AF5q31$^{+/+}$, AF5q31$^{+/-}$, and AF5q31$^{-/-}$ mice (68, 69).

One report demonstrated that AF5q31 is associated with P-TEFb and may contribute to regulate RNAPII processivity by phosphorylation of the CTD (20). To monitor RNAPII phosphorylation in MEFs derived from AF5q31$^{+/+}$, AF5q31$^{+/-}$, and AF5q31$^{-/-}$ embryos, we did Western blotting with antibodies N20, H5, and H14 that recognize both the IIo and IIa RNAPII, Ser2, and Ser5 CTD phosphopeptides of RNAPII, respectively. Although the IIo form predominantly existed in MEFs, the proportion of the IIo to IIa form was not distinctly changed among AF5q31$^{+/+}$, AF5q31$^{+/-}$, and AF5q31$^{-/-}$ MEFs (Fig. 6E). The reason for this may relate to the compensation by other factors, including AF4, LAF4, and FMR2, in the absence of AF5q31. To assess the effect of AF5q31 on P-TEFb, an in vitro kinase assay was performed using reconstitution proteins. To obtain a sufficient quantity of AF5q31 for further biochemical studies, whole-cell lysates of Sf9 cells expressing epitope-tagged AF5q31 (N-terminal HA tag and C-terminal FLAG tag) were purified by immunoaffinity chromatography using anti-Flag and anti-HA antibody columns, successively. Epitope-tagged AF5q31 proteins were allowed to bind to a Mono Q column and were then eluted with a linear gradient from 200 mM to 400 mM KCl (Fig. 6F, upper panel). Fractions peaking from 320 to 380 mM KCl (fractions 7 to 9) were found to contain AF5q31. The activities of each eluate were compared by the CTD in vitro kinase assay (66, 67). However, the CTD phosphorylations corresponding to fractions 7 to 9 were not significantly changed from those corresponding to the other fractions (Fig. 6F, lower panel). These results suggested that AF5q31 regulates spermiogenesis through the modulation of tissue-specific gene expression in Sertoli cells rather than affecting general transcriptional machinery.

Germ cell apoptosis in AF5q31$^{-/-}$ mice. To further clarify why AF5q31$^{-/-}$ mice were infertile and azoospermatic, the frequency of apoptotic cells in testes was compared between AF5q31$^{+/+}$ and AF5q31$^{-/-}$ mice by using a TUNEL assay (Fig. 7A). This assay revealed a 6.5-fold increase in apoptotic germ cells in seminiferous tubules in 12-week-old mutant mice, yet these were barely detectable in wild-type littermates (Fig. 7B). Hence, AF5q31 appears to be essential in both the differentiation program and the survival of germ cells.

DISCUSSION

Incomplete penetrance of the embryonic and neonatal lethality observed in AF5q31-deficient mice indicates that the

loss of AF5q31 does not cause a complete and uniform block of embryogenesis at a given point but that AF5q31 possesses versatile roles during embryogenesis. Since *AF5q31* and *AF4* are widely expressed during embryogenesis and in the adult tissues of mice, it is possible that AF4 functionally compensates for the lack of AF5q31 in most tissues (4, 33). Presently, it is unclear why the embryonic and neonatal death occurs and whether the incomplete penetrance of this phenotype results from heterogeneity in the genetic background of the mutant mice.

Spermatogenesis is a multistep process from spermatogonia, which are the stem cells of the germ cell lineage, to spermatozoa (14). Sertoli cells play major roles in supporting spermatogenesis, which involves the complex interaction of germ cells and Sertoli cells within the seminiferous tubules (23, 62), and Leydig cells produce the testosterone. The expression of AF5q31 in Sertoli cells without the expression of other family genes in the testis suggests an indispensable role for AF5q31 in the testis. It should be kept in mind that serum levels of testosterone, LH, and FSH and expression levels of *AR*, *LH-R*, and *FSH-R* did not show any significant difference between the wild-type and AF5q31$^{-/-}$ mice. Thus, azoospermia in AF5q31$^{-/-}$ mice seems to be caused by functional defects in testicular somatic cells, particularly Sertoli cells. Several reports suggested that abnormal Sertoli cells were impaired regarding the ability to assist the normal maturation and release of spermatids in the deficient mice for the nuclear receptors and related cofactors such as *RARα*, *RXRβ*, *AR*, and *Cnot7* (10, 15, 30, 36, 40, 48). It is possible that AF5q31 functions as a coregulator of these transcription factors in spermatogenesis.

Human infertility affects 10 to 15% of couples, with an approximately equal contribution from both partners (16). In a large number of male infertility patients, the cause of the infertility might be related to disturbances in the replacement of histones by protamines during spermatogenesis. Previous reports stated that sperm from sterile males shows abnormal protein contents, with anomalously elevated levels of histones and/or an altered protamine 1/2 ratio (3, 11, 17). In mice and humans, genes encoding *Prm1*, *Prm2*, and *TP2* are clustered together on chromosome 16 (52). In addition, these three genes lie in the same orientation to one another and are coordinately expressed in a haploid-specific manner during spermatogenesis. Notwithstanding the subtle decrease of *TP1* expression, the levels of *TP2*, *Prm1*, and *Prm2* were dramatically reduced in AF5q31$^{-/-}$ mice. Previous studies demonstrated that the transcription of transition proteins and protamines initiates shortly after the completion of meiosis in round spermatids (after step 7 in spermiogenesis) and ceases in elongating spermatids (step 11) with a global repression of transcription (37, 42). In addition, the haplo-insufficient chimeras of *Prm1* and *Prm2* were infertile, displaying an abnormal nuclear condensation (12). Thus, the reduced levels of TP2, Prm1, and Prm2 may be the cause of spermiogenesis arrest in AF5q31$^{-/-}$ mice.

Selective decreases in the levels of mRNAs of *TP2*, *Prm1*, and *Prm2* among a set of postmeiotic genes in germ cells raise the possibility that AF5q31 also directly regulates the transcription of these genes. In fact, AF5q31 is weakly expressed in germ cells. It remains to be determined if Sertoli cells and germ cells are independently affected by the lack of AF5q31 or

whether germ cells are secondarily affected, or both. Clarification of a potential role for AF5q31 in regulating the expression levels of *TP2*, *Prm1*, and *Prm2* may provide new insights into the mechanisms of human male infertility.

ALLs are characterized by the clonal proliferation, accumulation, and tissue infiltration of neoplastic cells (21). The majority of cases of ALL demonstrate abnormal karyotypes, either in chromosome number or as structural changes such as translocations, inversions, or deletions. As a consequence of translocations between chromosomes 5 and 11, the reciprocal fusion gene is generated and it encodes the MLL-AF5q31 fusion protein, which is expressed in the leukemic blasts (63). It is unknown whether the fusion protein can act as a dominant negative product on AF5q31 function in the leukemic blasts. However, the fact that AF5q31$^{-/-}$ mice did not show any hematological abnormalities suggests that the dominant negative effects of this fusion protein on AF5q31 in leukemogenesis are less likely. It is more likely that MLL-AF5q31 fusion leads to constitutive activation of the MLL target genes (1, 27). Clarification of the AF5q31-mediated gene regulation in testes will also help us to elucidate the molecular mechanism by which the fusion converts normal MLL into the leukemogenic form.

REFERENCES

1. **Armstrong, S. A., J. E. Staunton, L. B. Silverman, R. Pieters, M. L. den Boer, M. D. Minden, S. E. Sallan, E. S. Lander, T. R. Golub, and S. J. Korsmeyer.** 2002. MLL translocations specify a distinct gene expression profile that distinguishes a unique leukemia. Nat. Genet. **30**:41–47.
2. **Ayton, P. M., and M. L. Cleary.** 2001. Molecular mechanisms of leukemogenesis mediated by MLL fusion proteins. Oncogene **20**:5695–5707.
3. **Balhorn, R., S. Reed, and N. Tanphaichitr.** 1988. Aberrant protamine 1/protamine 2 ratios in sperm of infertile human males. Experientia **44**:52–55.
4. **Baskaran, K., F. Erfurth, G. Taborn, N. G. Copeland, D. J. Gilbert, N. A. Jenkins, P. M. Iannaccone, and P. H. Domer.** 1997. Cloning and developmental expression of the murine homolog of the acute leukemia proto-oncogene AF4. Oncogene **15**:1967–1978.
5. **Blendy, J. A., K. H. Kaestner, G. F. Weinbauer, E. Nieschlag, and G. Schutz.** 1996. Severe impairment of spermatogenesis in mice lacking the CREM gene. Nature **380**:162–165.
6. **Bursen, A., S. Moritz, A. Gaussmann, S. Moritz, T. Dingermann, and R. Marschalek.** 2004. Interaction of AF4 wild-type and AF4.MLL fusion protein with SIAH proteins: indication for t(4;11) pathobiology? Oncogene **23**:6237–6249.
7. **Canaani, E., P. C. Nowell, and C. M. Croce.** 1995. Molecular genetics of 11q23 chromosome translocations. Adv. Cancer Res. **66**:213–234.
8. **Chakrabarti, L., S. J. Knight, A. V. Flannery, and K. E. Davies.** 1996. A candidate gene for mild mental handicap at the FRAXE fragile site. Hum. Mol. Genet. **5**:275–282.
9. **Chakrabarti, L., J. Bristulf, G. S. Foss, and K. E. Davies.** 1998. Expression of the murine homologue of FMR2 in mouse brain and during development. Hum. Mol. Genet. **7**:441–448.
10. **Chang, C., Y. T. Chen, S. D. Yeh, Q. Xu, R. S. Wang, F. Guillou, H. Lardy, and S. Yeh.** 2004. Infertility with defective spermatogenesis and hypotestosteronemia in male mice lacking the androgen receptor in Sertoli cells. Proc. Natl. Acad. Sci. USA **101**:6876–6881.
11. **Chevaillier, P., N. Mauro, D. Feneux, P. Jouannet, and G. David.** 1987. Anomalous protein complement of sperm nuclei in some infertile men. Lancet **2**:806–807.
12. **Cho, C., W. D. Willis, E. H. Goulding, H. Jung-Ha, Y. C. Choi, N. B. Hecht, and E. M. Eddy.** 2001. Haploinsufficiency of protamine-1 or -2 causes infertility in mice. Nat. Genet. **28**:82–86.

13. Collins, E. C., and T. H. Rabbitts. 2002. The promiscuous MLL gene links chromosomal translocations to cellular differentiation and tumour tropism. Trends Mol. Med. 8:436–442.

14. Cooke, H. J., and P. T. Saunders. 2002. Mouse models of male infertility. Nat. Rev. Genet. 3:790–801.

15. De Gendt, K., J. V. Swinnen, P. T. Saunders, L. Schoonjans, M. Dewerchin, A. Devos, K. Tan, N. Atanassova, F. Claessens, C. Lecureuil, W. Heyns, P. Carmeliet, F. Guillou, R. M. Sharpe, and G. Verhoeven. 2004. A Sertoli cell-selective knockout of the androgen receptor causes spermatogenic arrest in meiosis. Proc. Natl. Acad. Sci. USA 101:1327–1332.

16. De Kretser, D. M., and H. W. Baker. 1999. Infertility in men: recent advances and continuing controversies. J. Clin. Endocrinol. Metab. 84:3443–3450.

17. de Yebra, L., J. L. Ballesca, J. A. Vanrell, L. Bassas, and R. Oliva. 1993. Complete selective absence of protamine P2 in humans. J. Biol. Chem. 268:10553–10557.

18. Djabali, M., L. Selleri, P. Parry, M. Bower, B. D. Young, and G. A. Evans. 1992. A trithorax-like gene is interrupted by chromosome 11q23 translocations in acute leukaemias. Nat. Genet. 2:113–118.

19. Domer, P. H., S. S. Fakharzadeh, C. S. Chen, J. Jockel, L. Johansen, G. A. Silverman, J. H. Kersey, and S. J. Korsmeyer. 1993. Acute mixed-lineage leukemia t(4;11)(q21;q23) generates an MLL-AF4 fusion product. Proc. Natl. Acad. Sci. USA 90:7884–7888.

20. Estable, M. C., M. H. Naghavi, H. Kato, H. Xiao, J. Qin, A. Vahlne, and R. G. Roeder. 2002. MCEF, the newest member of the AF4 family of transcription factors involved in leukemia, is a positive transcription elongation factor-b-associated protein. J. Biomed. Sci. 9:234–245.

21. Faderl, S., H. M. Kantarjian, M. Talpaz, and Z. Estrov. 1998. Clinical significance of cytogenetic abnormalities in adult acute lymphoblastic leukemia. Blood 91:3995–4019.

22. Gecz, J., A. K. Gedeon, G. R. Sutherland, and J. C. Mulley. 1996. Identification of the gene FMR2, associated with FRAXE mental retardation. Nat. Genet. 13:105–108.

23. Griswold, M. D. 1995. Interactions between germ cells and Sertoli cells in the testis. Biol. Reprod. 52:211–216.

24. Gu, Y., T. Nakamura, H. Alder, R. Prasad, O. Canaani, G. Cimino, C. M. Croce, and E. Canaani. 1992. The t(4;11) chromosome translocation of human acute leukemias fuses the ALL-1 gene, related to Drosophila trithorax, to the AF-4 gene. Cell 71:701–708.

25. Gu, Y., Y. Shen, R. A. Gibbs, and D. L. Nelson. 1996. Identification of FMR2, a novel gene associated with the FRAXE CCG repeat and CpG island. Nat. Genet. 13:109–113.

26. Guerif, F., V. Cadoret, M. Plat, M. Magistrini, J. Lansac, M. T. Hochereau-De Reviers, and D. Royere. 2002. Characterization of the fertility of Kit haplodeficient male mice. Int. J. Androl. 25:358–368.

27. Hess, J. L. 2004. MLL: a histone methyltransferase disrupted in leukemia. Trends Mol. Med. 10:500–507.

28. Hillman, M. A., and J. Gecz. 2001. Fragile XE-associated familial mental retardation protein 2 (FMR2) acts as a potent transcription activator. J. Hum. Genet. 46:251–259.

29. Hiwatari, M., T. Taki, T. Taketani, M. Taniwaki, K. Sugita, M. Okuya, M. Eguchi, K. Ida, and Y. Hayashi. 2003. Fusion of an AF4-related gene, LAF4, to MLL in childhood acute lymphoblastic leukemia with t(2;11)(q11;q23). Oncogene 22:2851–2855.

30. Holdcraft, R. W., and R. E. Braun. 2004. Androgen receptor function is required in Sertoli cells for the terminal differentiation of haploid spermatids. Development 131:459–467.

31. Huret, J. L., P. Dessen, and A. Bernheim. 2001. An atlas of chromosomes in hematological malignancies. Example: 11q23 and MLL partners. Leukemia 15:987–989.

32. Isaacs, A. M., P. L. Oliver, E. L. Jones, A. Jeans, A. Potter, B. H. Hovik, P. M. Nolan, L. Vizor, P. Glenister, A. K. Simon, I. C. Gray, N. K. Spurr, S. D. Brown, A. J. Hunter, and K. E. Davies. 2003. A mutation in Af4 is predicted to cause cerebellar ataxia and cataracts in the robotic mouse. J. Neurosci. 23:1631–1637.

33. Isnard, P., D. Depetris, M. G. Mattei, P. Ferrier, and M. Djabali. 1998. cDNA cloning, expression and chromosomal localization of the murine AF-4 gene involved in human leukemia. Mamm. Genome 9:1065–1068.

34. Isnard, P., N. Core, P. Naquet, and M. Djabali. 2000. Altered lymphoid development in mice deficient for the mAF4 proto-oncogene. Blood 96:705–710.

35. Kashiwabara, S., J. Noguchi, T. Zhuang, K. Ohmura, A. Honda, S. Sugiura, K. Miyamoto, S. Takahashi, K. Inoue, A. Ogura, and T. Baba. 2002. Regulation of spermatogenesis by testis-specific, cytoplasmic poly(A) polymerase TPAP. Science 298:1999–2002.

36. Kastner, P., M. Mark, M. Leid, A. Gansmuller, W. Chin, J. M. Grondona, D. Decimo, W. Krezel, A. Dierich, and P. Chambon. 1996. Abnormal spermatogenesis in RXR beta mutant mice. Genes Dev. 10:80–92.

37. Kierszenbaum, A. L., and L. L. Tres. 1975. Structural and transcriptional features of the mouse spermatid genome. J. Cell Biol. 65:258–270.

38. Kurohmaru, M., Y. Kanai, and Y. Hayashi. 1992. A cytological and cytoskeletal comparison of Sertoli cells without germ cell and those with germ cells using the W/W^v mutant mouse. Tissue Cell 24:895–903.

39. Kuzin, B., S. Tillib, Y. Sedkov, L. Mizrokhi, and A. Mazo. 1994. The Drosophila trithorax gene encodes a chromosomal protein and directly regulates the region-specific homeotic gene fork head. Genes Dev. 8:2478–2490.

40. Lufkin, T., D. Lohnes, M. Mark, A. Dierich, P. Gorry, M. P. Gaub, M. LeMeur, and P. Chambon. 1993. High postnatal lethality and testis degeneration in retinoic acid receptor alpha mutant mice. Proc. Natl. Acad. Sci. USA 90:7225–7229.

41. Ma, C., and L. M. Staudt. 1996. LAF-4 encodes a lymphoid nuclear protein with transactivation potential that is homologous to AF-4, the gene fused to MLL in t(4;11) leukemias. Blood 87:734–745.

42. Mali, P., A. Kaipia, M. Kangasniemi, J. Toppari, M. Sandberg, N. B. Hecht, and M. Parvinen. 1989. Stage-specific expression of nucleoprotein mRNAs during rat and mouse spermiogenesis. Reprod. Fertil. Dev. 1:369–382.

43. Martianov, I., G. M. Fimia, A. Dierich, M. Parvinen, P. Sassone-Corsi, and I. Davidson. 2001. Late arrest of spermiogenesis and germ cell apoptosis in mice lacking the TBP-like TLF/TRF2 gene. Mol. Cell 7:509–515.

44. Mazo, A. M., D. H. Huang, B. A. Mozer, and I. B. Dawid. 1990. The trithorax gene, a trans-acting regulator of the bithorax complex in Drosophila, encodes a protein with zinc-binding domains. Proc. Natl. Acad. Sci. USA 87:2112–2116.

45. Milne, T. A., S. D. Briggs, H. W. Brock, M. E. Martin, D. Gibbs, C. D. Allis, and J. L. Hess. 2002. MLL targets SET domain methyltransferase activity to Hox gene promoters. Mol. Cell 10:1107–1117.

46. Morrissey, J., D. C. Tkachuk, A. Milatovich, U. Francke, M. Link, and M. L. Cleary. 1993. A serine/proline-rich protein is fused to HRX in t(4;11) acute leukemias. Blood 81:1124–1131.

47. Mozer, B. A., and I. B. Dawid. 1989. Cloning and molecular characterization of the trithorax locus of Drosophila melanogaster. Proc. Natl. Acad. Sci. USA 86:3738–3742.

48. Nakamura, T., R. Yao, T. Ogawa, T. Suzuki, C. Ito, N. Tsunekawa, K. Inoue, R. Ajima, T. Miyasaka, Y. Yoshida, A. Ogura, K. Toshimori, T. Noce, T. Yamamoto, and T. Noda. 2004. Oligo-astheno-teratozoospermia in mice lacking Cnot7, a regulator of retinoid X receptor beta. Nat. Genet. 36:528–533.

49. Nakamura, T., H. Alder, Y., Gu, R. Prasad, O. Canaani, N. Kamada, R. P. Gale, B. Lange, W. M. Crist, and P. C. Nowell. 1993. Genes on chromosomes 4, 9, and 19 involved in 11q23 abnormalities in acute leukemia share sequence homology and/or common motifs. Proc. Natl. Acad. Sci. USA 90:4631–4635.

50. Nakamura, T., T. Mori, S. Tada, W. Krajewski, T. Rozovskaia, R. Wassell, G. Dubois, A. Mazo, C. M. Croce, and E. Canaani. 2002. ALL-1 is a histone methyltransferase that assembles a supercomplex of proteins involved in transcriptional regulation. Mol. Cell 10:1119–1128.

51. Nantel, F., L. Monaco, N. S. Foulkes, D. Masquilier, M. LeMeur, K. Henriksen, A. Dierich, M. Parvinen, and P. Sassone-Corsi. 1996. Spermiogenesis deficiency and germ-cell apoptosis in CREM-mutant mice. Nature 380:159–162.

52. Nelson, J. E., and S. A. Krawetz. 1993. Linkage of human spermatid-specific basic nuclear protein genes. Definition and evolution of the P1→P2→TP2 locus. J. Biol. Chem. 268:2932–2936.

53. Nilson, I., M. Reichel, M. G. Ennas, R. Greim, C. Knorr, G. Siegler, J. Greil, G. H. Fey, and R. Marschalek. 1997. Exon/intron structure of the human AF-4 gene, a member of the AF-4/LAF-4/FMR-2 gene family coding for a nuclear protein with structural alterations in acute leukaemia. Br. J. Haematol. 98:157–169.

54. Nosaka, T., J. M. van Deursen, R. A. Tripp, W. E. Thierfelder, B. A. Witthuhn, A. P. McMickle, P. C. Doherty, G. C. Grosveld, and J. N. Ihle. 1995. Defective lymphoid development in mice lacking Jak3. Science 270:800–802.

55. Nosaka, T., S. Morita, H. Kitamura, H. Nakajima, F. Shibata, Y. Morikawa, Y. Kataoka, Y. Ebihara, T. Kawashima, T. Itoh, K. Ozaki, E. Senba, K. Tsuji, F. Makishima, N. Yoshida, and T. Kitamura. 2003. Mammalian twisted gastrulation is essential for skeleto-lymphogenesis. Mol. Cell. Biol. 23:2969–2980.

56. Nosaka, T., T. Kawashima, K. Misawa, K. Ikuta, A. L.-F. Mui, and T. Kitamura. 1999. STAT5 as a molecular regulator of proliferation, differentiation and apoptosis in hematopoietic cells. EMBO J. 18:4654–4765.

57. Oliver, P. L., E. Bitoun, J. Clark, E. L. Jones, and K. E. Davies. 2004. Mediation of Af4 protein function in the cerebellum by Siah proteins. Proc. Natl. Acad. Sci. USA 101:14901–14906.

58. Prasad, R., T. Yano, C. Sorio, T. Nakamura, R. Rallapalli, Y. Gu, D. Leshkowitz, C. M. Croce, and E. Canaani. 1995. Domains with transcriptional regulatory activity within the ALL1 and AF4 proteins involved in acute leukemia. Proc. Natl. Acad. Sci. USA 92:12160–12164.

59. Rabbitts, T. H. 1994. Chromosomal translocations in human cancer. Nature 372:143–149.

60. Rowley, J. D. 2001. Chromosome translocations: dangerous liaisons revisited. Nat. Rev. Cancer 1:245–250.

61. Sassone-Corsi, P. 2002. Unique chromatin remodeling and transcriptional regulation in spermatogenesis. Science 296:2176–2178.

62. Siu, M. K., and C. Y. Cheng. 2004. Dynamic cross-talk between cells and the extracellular matrix in the testis. Bioessays 26:978–992.

63. Taki, T., H. Kano, M. Taniwaki, M. Sako, M. Yanagisawa, and Y. Hayashi.

1999. AF5q31, a newly identified AF4-related gene, is fused to MLL in infant acute lymphoblastic leukemia with ins(5;11)(q31;q13q23). Proc. Natl. Acad. Sci. USA 96:14535–14540.

64. Tkachuk, D. C., S. Kohler, and M. L. Cleary. 1992. Involvement of a homolog of Drosophila trithorax by 11q23 chromosomal translocations in acute leukemias. Cell 7:691–700.

65. von Bergh, A. R., H. B. Beverloo, P. Rombout, E. R. van Wering, M. H. van Weel, G. C. Beverstock, P. M. Kluin, R. M. Slater, and E. Schuuring. 2002. LAF4, an AF4-related gene, is fused to MLL in infant acute lymphoblastic leukemia. Genes Chromosomes Cancer 35:92–96.

66. Wada, T., T. Takagi, Y. Yamaguchi, A. Ferdous, T. Imai, S. Hirose, S. Sugimoto, K. Yano, G. A. Hartzog, F. Winston, S. Buratowski, and H. Handa. 1998. DSIF, a novel transcription elongation factor that regulates RNA polymerase II processivity, is composed of human Spt4 and Spt5 homologs. Genes Dev. 12:343–356.

67. Wada, T., T. Takagi, Y. Yamaguchi, D. Watanabe, and H. Handa. 1998. Evidence that P-TEFb alleviates the negative effect of DSIF on RNA polymerase II-dependent transcription in vitro. EMBO J. 17:7395–7403.

68. Wu, J. Y., and A. R. Means. 2000. Ca(2+)/calmodulin-dependent protein kinase IV is expressed in spermatids and targeted to chromatin and the nuclear matrix. J. Biol. Chem. 275:7994–7999.

69. Wu, J. Y., T. J. Ribar, D. E. Cummings, K. A. Burton, G. S. McKnight, and A. R. Means. 2000. Spermiogenesis and exchange of basic nuclear proteins are impaired in male germ cells lacking Camk4. Nat. Genet. 25:448–452.

70. Yokoyama, A., Z. Wang, J. Wysocka, M. Sanyal, D. J. Aufiero, I. Kitabayashi, W. Herr, and M. L. Cleary. 2004. Leukemia proto-oncoprotein MLL forms a SET1-like histone methyltransferase complex with menin to regulate Hox gene expression. Mol. Cell. Biol. 24:5639–5649.

71. Yomogida, K., H. Ohtani, H. Harigae, E. Ito, Y. Nishimune, J. D. Engel, and M. Yamamoto. 1994. Developmental stage- and spermatogenic cycle-specific expression of transcription factor GATA-1 in mouse Sertoli cells. Development 120:1759–1766.

72. Yu, B. D., J. L. Hess, S. E. Horning, G. A. Brown, and S. J. Korsmeyer. 1995. Altered Hox expression and segmental identity in Mll-mutant mice. Nature 378:505–508.

73. Yu, B. D., R. D. Hanson, J. L. Hess, S. E. Horning, and S. J. Korsmeyer. 1998. MLL, a mammalian trithorax-group gene, functions as a transcriptional maintenance factor in morphogenesis. Proc. Natl. Acad. Sci. USA 95:10632–10636.

74. Zhang, D., T. L. Penttila, P. L. Morri, M. Teichmann, and R. G. Roeder. 2001. Spermiogenesis deficiency in mice lacking the Trf2 gene. Science 292:1153–1155.